Dartmouth College

Dartmouth Digital Commons

2-11-2014

Tracing the Evolution of Active Galactic Nuclei Host Galaxies Over The Last 9 Gyr of Cosmic Time

A. D. Goulding
Harvard-Smithsonian Center for Astrophysics

W. R. Forman
Harvard-Smithsonian Center for Astrophysics

R. C. Hickox
Dartmouth College

C. Jones
Harvard-Smithsonian Center for Astrophysics

Recommended Citation

TRACING THE EVOLUTION OF ACTIVE GALACTIC NUCLEI HOST GALAXIES OVER THE LAST 9 Gyr OF COSMIC TIME

A. D. Goulding[1], W. R. Forman[1], R. C. Hickox[2], C. Jones[1], S. S. Murray[1,3], A. Paggi[1], M. L. N. Ashby[1],
A. L. Coil[4], M. C. Cooper[5], J.-S. Huang[1], R. Kraft[1], J. A. Newman[6], B. J. Weiner[7], and S. P. Willner[1]

[1] Harvard-Smithsonian Center for Astrophysics, 60 Garden Street, Cambridge, MA 02138, USA; agoulding@cfa.harvard.edu
[2] Department of Physics and Astronomy, Dartmouth College, Hanover, NH 03755, USA
[3] Department of Physics and Astronomy, Johns Hopkins University, 3400 North Charles Street, Baltimore, MD 21218, USA
[4] Department of Physics, Center for Astrophysics and Space Sciences, University of California at San Diego,
9500 Gilman Drive, La Jolla, San Diego, CA 92093, USA
[5] Center for Galaxy Evolution, Department of Physics and Astronomy, University of California, Irvine,
4129 Frederick Reines Hall, Irvine, CA 92697, USA
[6] Department of Physics and Astronomy, University of Pittsburgh, 3941 O'Hara Street, Pittsburgh, PA 15260, USA
[7] Steward Observatory, 933 North Cherry Street, University of Arizona, Tucson, AZ 85721, USA

ABSTRACT

We present the results of a combined galaxy population analysis for the host galaxies of active galactic nuclei (AGN) identified at $0 < z < 1.4$ within the Sloan Digital Sky Survey, Boötes, and DEEP2 surveys. We identified AGN in a uniform and unbiased manner at X-ray, infrared, and radio wavelengths. Supermassive black holes undergoing radiatively efficient accretion (detected as X-ray and/or infrared AGN) appear to be hosted in a separate and distinct galaxy population than AGN undergoing powerful mechanically dominated accretion (radio AGN). Consistent with some previous studies, radiatively efficient AGN appear to be preferentially hosted in modest star-forming galaxies, with little dependence on AGN or galaxy luminosity. AGN exhibiting radio-emitting jets due to mechanically dominated accretion are almost exclusively observed in massive, passive galaxies. Crucially, we now provide strong evidence that the observed host-galaxy trends are independent of redshift. In particular, these different accretion-mode AGN have remained as separate galaxy populations throughout the last 9 Gyr. Furthermore, it appears that galaxies hosting AGN have evolved along the same path as galaxies that are not hosting AGN with little evidence for distinctly separate evolution.

Key words: galaxies: active – galaxies: evolution – galaxies: statistics – infrared: galaxies – radio continuum: galaxies – surveys – X-rays: galaxies

Online-only material: color figures

1. INTRODUCTION

Accreting supermassive black holes (BHs) in the form of active galactic nuclei (AGN) are capable of releasing enormous quantities of energy over their lifetimes, often comparable to the binding energy of their host galaxies ($> 10^{61}$ erg; for a review, see Alexander & Hickox 2012). In light of this, many theoretical and semi-analytical galaxy evolution simulations now incorporate AGN feedback processes as a form of self-regulation for BH growth and star formation. It is predicted that major mergers between gas-rich galaxies drive nuclear inflows, which trigger powerful starbursts and fuel the growth of central BHs (Di Matteo et al. 2005; Hopkins et al. 2007, 2008; Menci et al. 2008). In turn, these models often reproduce key observables such as the bulge–BH mass scaling relations (e.g., Magorrian et al. 1998; Tremaine et al. 2002) and the observed luminosity functions of quasars and normal galaxies (e.g., Richards et al. 2006; Ross et al. 2013).

Despite the success of current models, it is now becoming clear that galaxy–galaxy mergers, which are required by some of the cosmological simulations, are relatively rare events and may not be driving the bulk of galaxy and AGN co-evolution (for a recent review of AGN/galaxy co-evolution, see Kormendy & Ho 2013). Indeed, dedicated multiwavelength (optical; X-ray; far-infrared) studies are providing mounting evidence that the majority of AGN–galaxy co-evolution is dominated by more secular processes (i.e., due to material accreted directly from the host galaxy). Analysis of the distribution of AGN morphologies

and their position in galaxy color versus absolute magnitude space shows that at $z \sim 1$–2, AGN hosts are predominantly star-forming and disk-dominated ("blue-cloud") galaxies and not merging systems (e.g., Georgakakis et al. 2009; Schawinski et al. 2011; Cisternas et al. 2011; Mullaney et al. 2012; Rosario et al. 2012). There have been suggestions that relatively isolated X-ray AGN may represent a specific population of galaxies that are undergoing a transition in their stellar and morphological properties (e.g., Nandra et al. 2007; Coil et al. 2009; Hickox et al. 2009; Xue et al. 2010), and this transition is due to the central AGN. The most extreme cases of this transition population may be due to the presence of a luminous quasar with accretion in excess of 10% of the Eddington rate. A quasar phase is expected to rapidly truncate ongoing star formation by driving out the available cool gas supply in the form of a disk wind that is radiatively efficient (see Fabian 2012 for a review). Such a rapid BH growth stage may (in part) provide a feedback mechanism to evolve blue galaxies onto the red sequence (e.g., Hopkins & Elvis 2010).

Unlike radiatively efficient AGN and quasars that are ubiquitously detected in optical/IR/X-ray surveys, radio AGN, which accrete matter through advection-dominated processes, are almost exclusively hosted in old stellar population (red sequence) massive spheroidal galaxies (e.g., Best et al. 2005; Kauffmann et al. 2008). These red-sequence galaxies are expected to have evolved through catastrophic interactions such as major mergers. The most powerful radio sources are often hosted in massive spheroidal systems cocooned within hot atmospheres, such as

those at the centers of galaxy clusters and dense groups. The mechanical energy released by the central radio source is injected back into the interstellar and intracluster medium (so-called radio-mode feedback), reducing the production of new stars in these massive (gas-rich) systems. Tracing the hosts of these two fundamentally different accretion mode (radiatively efficient versus advection-dominated) AGN populations during the epoch where the red sequence of galaxies is forming (Bell et al. 2004; Borch et al. 2006; Faber et al. 2007) may provide valuable insight into galaxy evolution and AGN feedback.

Wide-field spectroscopic surveys that include tens to hundreds of thousands of extragalactic sources have shown that the galaxy luminosity and stellar-mass functions evolve strongly from $z \sim 1.5$ to the present day, with the main build-up of the red sequence occurring since $z \sim 1$ (Bell et al. 2004; Borch et al. 2006; Cooper et al. 2006; Faber et al. 2007; Moustakas et al. 2013). Clearly, $z \sim 1$ is an important epoch to study the interaction between growing supermassive BHs and their hosts. The accurate identification and selection of relatively distant galaxies and AGN requires robust source redshift measurements. Indeed, to constrain the color distributions and evolution of the AGN hosts, accurate spectroscopic redshift measurements are required to break the degeneracy between inferred properties (such as star formation history, stellar mass, and color) and redshift that is inherent in photometric redshift determinations, particularly for surveys with limited multiwavelength narrow-band photometric coverage.

In the nearby universe ($z < 0.2$), surveys such as the Sloan Digital Sky Survey and 2dF Galaxy Redshift Survey have provided an unprecedented wealth of spectroscopic data across $\sim 10,000$ deg^2 (in extragalactic sky regions), which has been used effectively to identify and understand the optical, radio, and to some extent, the X-ray and infrared (IR) properties of AGN and galaxies locally (e.g., Kauffmann et al. 2003a; Heckman et al. 2004; LaMassa et al. 2009, 2012; Shao et al. 2013). However, while useful for selecting AGN in nearby galaxies (to $z < 0.2$), due to brightness limitations (e.g., including only galaxies with $r < 17.77$ in the SDSS), these surveys sample only the most luminous and massive systems at higher redshifts ($z > 0.2$). Furthermore, it has now been widely established that no single waveband can accurately provide a complete sample of AGN due primarily to (1) absorption/obscuration of the central BH; (2) contamination by the host galaxy (e.g., Hickox et al. 2009; Hopkins et al. 2009; Donley et al. 2010; Goulding et al. 2012a; Mendez et al. 2013); and (3) individual wavebands preferentially selecting particular accretion mechanisms (i.e., radiative versus advection-dominated flows).

To trace the evolution of the typical population of AGN and their hosts to $z \sim 1.4$ within similar and unbiased volume slices, we require a combination of relatively wide-field, sensitive multiwavelength (optical; radio; X-ray; IR) surveys with complete homogeneous spectroscopic coverage. Hence, here we harness the extensive datasets in three wide and blank field surveys with complete homogeneous optical spectroscopic coverage: the Sloan Digital Sky Survey ($z \sim 0$–0.3; York et al. 2000), Boötes ($z \sim 0.25$–0.8; Murray et al. 2005; Kochanek et al. 2012), and DEEP Extragalactic Evolutionary Probe 2 (DEEP2; $z \sim 0.7$–1.4; Davis et al. 2003; Newman et al. 2013). The redshift and galaxy property information established using these surveys, combined with the AGN identified using the multiwavelength data, provides one of the most complete views of AGN activity and the host-galaxy interaction at $z < 1.4$. Here, we explore the following.

1. The multiwavelength incidence of AGN activity in optically selected galaxies.
2. The distribution and median rest-frame optical colors of AGN host galaxies.
3. The (non-)evolution of AGN host-galaxy colors throughout the last 9 Gyr.

Section 2 introduces the three survey fields used in this work and describes how our galaxy sample was constructed. The full description of the parent galaxy samples and how these are matched for the differing detection methods and sensitivity limits of the individual fields are provided in the Appendix. Section 3 presents the methodology for building a obscuration unbiased sample of AGN identified in the IR, X-ray, and radio domains. Section 4 discusses the general host-galaxy properties of radio, X-ray, and IR-detected AGN (i.e., advection-dominated versus radiatively efficient AGN), and we show that there appears to be little evidence for evolution in the galaxy colors for individual AGN populations in the last 9 Gyr. Section 5 outlines the impact of our findings on AGN feedback models. Finally, Section 6 summarizes our findings. Throughout the manuscript, we adopt a standard flat ΛCDM cosmology with $H_0 = 71$ km s^{-1} Mpc^{-1} and $\Omega_M = 0.3$.

2. GALAXY SAMPLE SELECTION

Our parent galaxy sample, defined at $z \sim 0.05$–1.4, is constructed from a combination of galaxies identified in the Seventh Data Release of the Sloan Digital Sky Survey (hereafter SDSS; York et al. 2000; Abazajian et al. 2009) at $0.05 < z < 0.2$, the NOAO Deep Wide-Field Survey Boötes field (Murray et al. 2005; Kochanek et al. 2012) at $0.2 < z < 0.7$, and the DEEP2 Galaxy Redshift Survey fields (Davis et al. 2003; Newman et al. 2013) at $0.7 < z < 1.4$. One of the primary aims of this experiment is to construct an unbiased like-for-like galaxy sample from which to explore the properties of galaxies hosting luminous AGN; i.e., the aim is to construct a large galaxy sample selected consistently in all three surveys, irrespective of the individual galaxy redshift, mass, color, luminosity, and rest-frame flux limit of the survey. Hence, given that the SDSS, Boötes, and DEEP2 surveys have different rest-frame photometric and spectroscopic selection techniques, we cannot simply use the full galaxy catalogs. The Appendix material provides a thorough explanation of our sample selection technique to match the galaxies identified in the three surveys according to passive evolution-corrected luminosity and spectral color across the entire redshift range explored here. Briefly, we built upon the previous methodology of Blanton (2006) and performed photometric K-corrections using the publicly available C and IDL tool, KCORRECT (v4.2).[8] These measurements were then matched to the initial galaxy catalogs based on their rest-frame optical measurements in accordance with the selection methodology of the surveys. We applied color and evolution corrections to each source and assigned two random redshifts drawn from the redshift distributions of the other two surveys. Those objects that are included in our final galaxy sample are sufficiently luminous (intrinsically) to be detected in all three parent surveys, independent of their specific observed redshift. Figure 1 provides a schematic flow diagram of the main processing steps and methodology for the sample selection procedure.

---

[8] The current version of KCORRECT is available at http://howdy.physics.nyu.edu/index.php/Kcorrect.
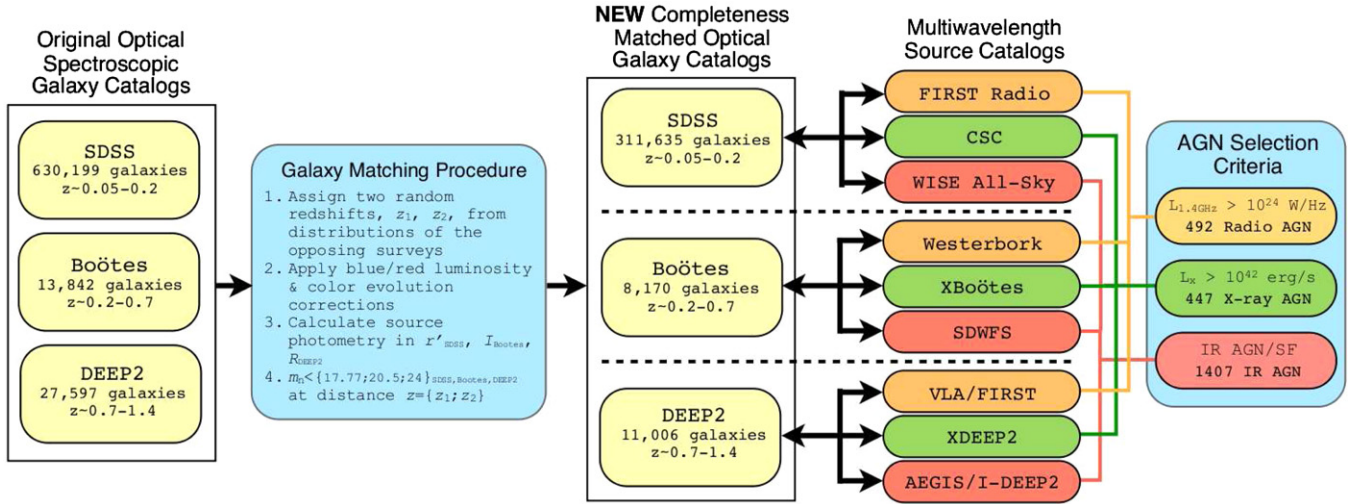
Figure 1. Schematic flow diagram highlighting the main steps in the construction of our relatively unbiased, optical-property-matched galaxy sample derived from the main SDSS-DR7, Boötes, and DEEP2 optical spectroscopic catalogs. Furthermore, we connect our matched galaxy sample, in each survey, to the appropriate multiwavelength catalogs to identify those galaxies hosting luminous AGN.

(A color version of this figure is available in the online journal.)

Table 1
Survey Properties

Survey	z	$m_{\rm limit}$ (AB Mag)	Gals with Spec-z in z-range	Completeness Matched Galaxies	Area (deg^2) Spec	X-ray	IR	Radio	No. of AGN X-ray	IR	Radio
(1)	(2)	(3)	(4)	(5)	(6)				(7)		
SDSS	0.05–0.2	$r < 17.77$	630,199	311,635 (~49%)	8032	130	8032	7550	73 (122[a])	1121	406
Boötes	0.2–0.7	$I < 20.5$	13,842	8,170 (~59%)	7.74	7.64	7.30	5.83	196	151	62
DEEP2	0.7–1.4	$R < 24.1$	27,597	11,006 (~40%)	2.78	2.66	1.64	2.78	178	135	24

Notes. (1) Survey field; DEEP2 = F1+F2+F3+F4. (2) Redshift range. (3) Brightness limit of the complete optical spectroscopic samples. (4) Number of sources with spectroscopic redshifts within the survey redshift range. (5) Number of sources in the completeness-limit-matched sample. (6) Spatial area of the spectroscopic survey in square degrees and the contiguous area covered by *Chandra* X-ray, *WISE* or *Spitzer* mid-IR and VLA or Westerbork radio photometry. (7) Number of AGN detected in the X-ray, IR, and radio from the matched source sample.
[a] X-ray AGN in SDSS with $L_X > 10^{41}$ erg s^{-1}.

Table 1 provides the source statistics, photometric limits, and redshift breakdowns for our color- and luminosity-matched galaxy samples across the three surveys. Those galaxies, included in the final-matched sample, have their templates deprojected into SDSS u and g filters in AB magnitudes. To aid comparison with previous studies (e.g., Blanton et al. 2003a, 2003b; Blanton 2006; Blanton & Roweis 2007; Kauffmann et al. 2003c; Hickox et al. 2009), the SDSS filters are shifted blueward to $z = 0.1$ and are defined as $^{0.1}u$ and $^{0.1}g$, respectively. Absolute magnitudes, including the passive evolution corrections, are calculated for each source. As is standard with KCORRECT, the absolute magnitudes are calculated assuming $h_0 = 1.0$, which we correct to $h_0 = 0.71$ to fit our assumed cosmology.

The top panel of Figure 2 shows the redshift distributions for our matched galaxy sample and for comparison purposes, the redshift distributions for the full galaxy samples in the SDSS, Boötes, and DEEP2 surveys. At $z < 0.7$, we find broadly similar redshift distributions between the main galaxy samples and our matched sample, suggesting that the matched sample is not overly biased from the main population. At $0.75 < z < 0.85$, there is an abundant population of galaxies that are present in the main DEEP2 survey but are not selected in our matched sample. These are low-luminosity $^{0.1}M_g > -19.5$ blue galaxies that are not selected in the matched sample due to the redder rest-frame wavelength selection in Boötes and the SDSS. The redshift distribution for the DEEP2 property-matched galaxies

is consistent with that expected when matched to Boötes and the SDSS. In the following sections, we identify galaxies that host AGN and use these samples to place constraints on the AGN host-galaxy properties.

3. AGN SAMPLE SELECTION

Many focused and blank field studies have shown that no one waveband can identify the full population of AGN (e.g., Martínez-Sansigre et al. 2007; Alexander et al. 2008; Donley et al. 2008; Hickox et al. 2009; Juneau et al. 2011; Trump et al. 2013; Mendez et al. 2013). For example, due to obscuration bias, optical surveys miss ≈50% of the AGN population (e.g., Goulding & Alexander 2009; Goulding et al. 2010), and even X-ray surveys, which are relatively unaffected by moderate levels of obscuration, still miss a significant fraction (~20%–50%) of AGN (e.g., Donley et al. 2005; Guainazzi et al. 2005; Park et al. 2010; Alexander et al. 2011; Georgantopoulos et al. 2013; Wilkes et al. 2013). To mitigate these biases, we harness the extensive multiwavelength data sets (*Spitzer*-IRAC; *WISE*; VLA-FIRST; *Chandra*-ACIS) falling in the SDSS, Boötes, and DEEP2 footprints.

The proceeding sections describe our methodology (similar to that of Hickox et al. 2009), for constructing a relatively large, obscuration-independent, unbiased AGN sample in the three survey regions (see also Figure 1). For radio and X-ray
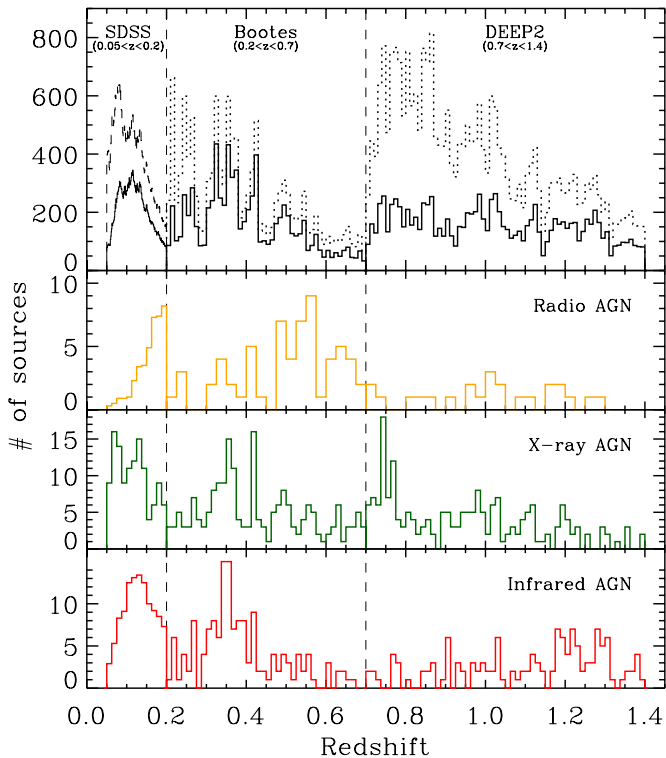
Figure 2. Top panel: spectral redshift distributions for the full parent catalogs (dashed line; SDSS-MPA-JHU; Kochanek et al. 2012; Newman et al. 2013) as well as the selection- and evolution-matched galaxy samples (solid line). The final-matched galaxy samples contain 311,685, 8170, and 11,006 sources in SDSS, Boötes, and DEEP2, respectively. Lower panels: spectral redshift distributions for AGN identified at radio (yellow solid), X-ray (green solid), and infrared (red solid) wavelengths in the survey fields. The histograms of the radio and IR AGN in the SDSS are scaled by a factor of 1/10 for presentation purposes.

(A color version of this figure is available in the online journal.)

AGN identification, we used a set of luminosity thresholds that are sufficiently high to remove luminous star-forming systems, while at infrared wavelengths, we employed a well-established AGN–star formation ratio diagnostic to identify less luminous (or obscured) AGN that are contributing significantly to the bolometric luminosity of their host galaxies. Furthermore, for a flux-limited sample, there is tendency to identify AGN in more massive galaxies (e.g., Aird et al. 2012). Hence, with the combination of the AGN selection methods/wavelength ranges used here, we can mitigate many potential baises and produce an almost complete and unbiased sample of AGN spread across a wide dynamic range in accretion rates, obscuration levels, and AGN luminosities.

3.1. Infrared AGN

Deep mid-IR surveys performed with the *WISE* and *Spitzer* observatories provide an almost obscuration-independent view of the universe and are now capable of resolving the bulk of the IR background at $\sim$3–70 μm (e.g., Dole et al. 2006; Frayer et al. 2006; Ashby et al. 2013). These pointed, wide-field, and all-sky surveys reveal large populations of dust-obscured starburst galaxies and AGN. By contrast to standard AGN detection methods (e.g., at radio; X-ray energies), which require a particular luminosity threshold that is unlikely to be produced by non-accretion processes, widely used IR AGN identification diagnostics are predicated on the contribution of the dust reradiated (intrinsic) AGN and star formation emission to the

bolometric luminosity of a particular galaxy. Such a diagnostic can often lead to the identification of more heavily dust-obscured AGN than would be found at other wavelengths, as both the AGN and the star formation can be obscured by dust located in the circumnuclear region, as well as the extended host galaxy.

3.1.1. WISE-selected AGN in the SDSS

The SDSS is covered in its entirety by the *WISE* mid-IR survey, providing four-band cryogenic photometry at 3.4, 4.6, 12, and 22 μm. We associated the SDSS sources with *WISE* counterparts using a similar procedure to the one presented by D'Abrusco et al. (2013), which we briefly recall here. For each SDSS source we searched for IR counterparts in the *WISE* all-sky archive within circular regions of variable radius R in the range between $0''$ and $4''$ with increment $\Delta R = 0''.1$. For each radial distance, we estimated the number of total ($N_t(R)$) and random ($N_r(R)$) matches together with the chance probability for the spurious associations $P(R)$. The random matches $N_r(R)$ correspond to those found by radially shifting the search region centroid by a randomized distance between $10''$ and $20''$. The chance probability for spurious associations $P(R)$ was calculated as the ratio between $N_r(R)$ and the total number of sources. We calculated the differences between the number of total matches at a given radius R and those at $R - \Delta R$ defined as $\Delta N_t(R) = N_t(R) - N_t(R - \Delta R)$, and the corresponding variation of the random associations, $\Delta N_r(R) = N_r(R) - N_r(R - \Delta R)$. At radii larger than $3''.1$, the increase in number of *WISE* sources that were positionally associated with a SDSS source was systematically lower than the increase in number of random associations. Thus, $3''.1$ was chosen as the radial threshold for searching for counterparts of SDSS sources in the *WISE* all-sky release. We identified 43,171 single *WISE* counterpart matches within $3''.1$ of an SDSS galaxy, 445 multiple matches, and 43,616 total matches, with a chance probability for spurious associations of $P(R < 3''.1) \sim 0.5\%$. For the 445 ($\sim$1% of the total) sources with multiple matches, we chose the counterpart with the smallest separation. The extra $\sim$0.5% of multiple source matches, over the expected $\sim$0.5% spurious matches is due to the non-random distribution of galaxies across the sky, i.e., galaxy clustering.

The majority of low-redshift extragalactic sources detected by *WISE* in the 3.4, 4.6, and 12 μm bands are dominated at mid-IR wavelengths by host-galaxy starlight. Based on a cross-correlation of SDSS and *WISE* galaxies, Yan et al. (2013) find that a significant proportion of optical emission-line classified AGN (based on BPT diagnostics) in the SDSS cannot be separated from their star-forming and low-ionization narrow emission-line region (LINER) galaxy counterparts using the typical *WISE* infrared [3.4]–[4.6] versus [4.6]–[12] color–color diagram. A large fraction of optical AGN, LINERs, and H II galaxies are predicted to reside close to the main locus at [4.6]–[12] $\sim$ 3.5 and [3.4]–[4.6] $\sim$ 0.25. However, based on the results of Yan et al. (2013), we may adopt the relatively conservative AGN selection criteria presented by Mateos et al. (2012) to select a mid-IR AGN sample that is expected to be free from contamination by H II galaxies and LINERs using the main SDSS-matched galaxy sample, shown in Figure 3(a). Of the 311,635 SDSS galaxies in our matched galaxy sample, 1121 are selected as AGN using the Mateos et al. (2012) *WISE* selection method. Figure 3(a) further confirms that the mid-IR AGN selection criteria is not subject to contamination from non-AGN systems. We predicted the color–color redshift tracks for a set of starburst, star-forming, spiral, and elliptical galaxies (see Donley
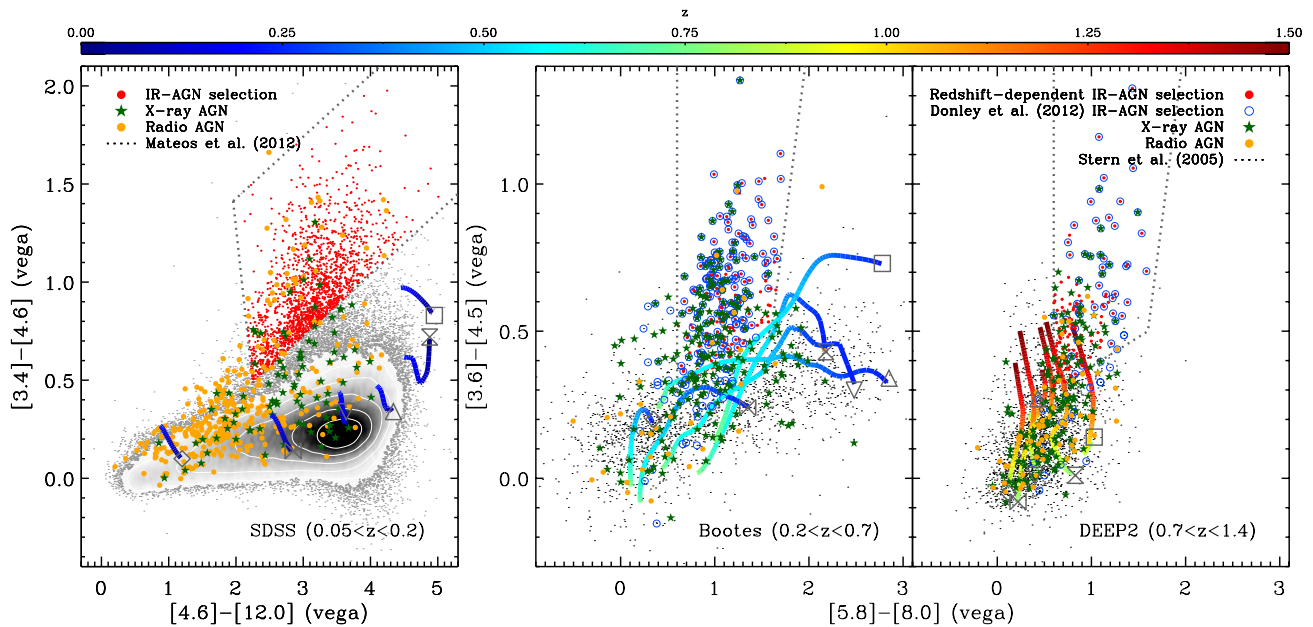
Figure 3. Redshift-dependent spectral tracks for starburst (square, hourglass), spiral (triangle, upturned triangle, bow-tie), and elliptical (diamond) galaxies are shown. Radio- and X-ray-detected AGN are shown with orange circles and green stars, respectively. Infrared color–color diagnostic-selected AGN are shown with red dots. Our choice of redshift-dependent AGN selection regions (see the main text) provides a clean AGN sample that does not included star-forming or passive galaxy (non-AGN) interlopers. (a) *WISE* infrared [3.4]–[4.6] vs. [4.6]–[12.0] Vega magnitude color–color selection of galaxies and AGN detected in the SDSS for sources at $0.05 < z < 0.2$ (contours and gray dots). The AGN (red circles) lying within the AGN diagnostic selection region of Mateos et al. (2012) is shown with dotted lines. (b) *Spitzer* IRAC infrared [3.6]–[4.5] vs. [5.8]–[8.0] Vega magnitude color–color selection of galaxies selected in the Boötes survey in the redshift range, $0.2 < z < 0.7$ (gray dots). Candidate AGN identified using the Stern et al. (2005; dotted region) and/or Donley et al. (2012; blue open circles) infrared AGN color selection methods are additionally shown. Infrared-selected AGN, after removal of star-forming interlopers, are shown with red filled circles. (c) Same as center panel except source sample is derived from the DEEP2 survey at $0.7 < z < 1.4$.

(A color version of this figure is available in the online journal.)

et al. 2012; hereafter D12). These tracks were calculated by convolving a set of infrared spectral energy distributions (SEDs) for the archetypal template galaxies (J. Donley 2013, private communication) with the *WISE* photometric filter responses to predict their *WISE* colors in the redshift range $z \sim 0.05$–0.2. None of these "non-AGN" template galaxies are expected to lie within, or close to, the *WISE* AGN selection region in the redshift range of the SDSS sample. Hence, our SDSS–*WISE* AGN sample can be considered a clean and conservative representation of the overall low-redshift IR AGN population.

3.1.2. Spitzer-IRAC-selected AGN in Boötes and DEEP2

Both the Boötes and DEEP2 surveys have dedicated infrared imaging campaigns performed using the *Spitzer* Infrared Array Camera (IRAC; Fazio et al. 2004) at 3.6, 4.5, 5.8, and 8.0 μm. The Boötes field is covered by the 8.5 deg^2 IRAC Shallow Survey (Eisenhardt et al. 2004) and the 10 deg^2 Spitzer Deep Wide-Field Survey (SDWFS; Ashby et al. 2009). The final SDWFS catalog includes ≈680,000 unique sources. The optical spectroscopic survey, AGES (Kochanek et al. 2012), covers ∼7.3 deg^2 of the SDWFS field. The spatially associated optical–IR source catalog exists as part of the AGES catalog, which we use here to provide the necessary IRAC photometry for AGN selection for our matched galaxy catalog in the Boötes field.

DEEP2 Fields 1, 2, and 4 have relatively complete four-band coverage with IRAC.[9] *Spitzer* IRAC Guaranteed Time Observations of DEEP2 Field 1 were performed as part of

the Extended Groth Strip (EGS) campaign. The IRAC–EGS observations cover a $10' \times 120'$ contiguous region across the center of the EGS survey and contain ∼57, 500 unique sources (Barmby et al. 2008). In addition, General Observing IRAC data were obtained for Fields 2 and 4 as part of Program 40689 PI G. Fazio and Program 50660 PI C. Jones. These four-band IRAC observations cover 0.92 deg^2 and 0.88 deg^2, respectively.

For consistency between the surveys, the *Spitzer* IRAC data were reduced following the method employed for the Boötes SDWFS observations (Ashby et al. 2009), which we briefly recall here. Basic calibrated data (BCD) images for the 3.6, 5.8, and 8.0 μm *Spitzer* IRAC observations were first post-processed using the MOPEX software package,[10] which removes data artifacts such as stray light, muxbleed, column pulldown, and banding and recalibrates the astrometry. The individual exposures were then object masked and median stacked. These stacked images were subtracted from the individual BCDs in each astronomical observation request to remove long-term residuals caused by previous observations of bright sources. This was not carried out for the 4.5 μm observations as the cryogenic 4.5 μm array does not suffer from residual effects. The individual image tiles were combined into full field mosaicked images, one for each band, using the Montage toolkit. After the masking of the bright stars present in the mosaicked images, sources were detected and extracted for each individual wavelength band using the standard tool, SExtractor (v2.50; Bertin & Arnouts 1996). To allow a closer comparison with the sources identified in the SDWFS data, we used SExtractor parameter settings identical to those presented in Table 2 of Ashby et al. (2009). This detection method was verified by generating background and object

---

[9] DEEP2 Field 3 has no current *Spitzer* IR photometry. For the purposes of homogeneity, as well as decreased sensitivity for distant objects, we do not include the available *WISE* photometry in DEEP2 Field 3 as this will potentially bias ensuing results to only the brightest systems, which may not be representative of the overall AGN/galaxy population.

[10] MOPEX is available from the Spitzer Science Center Web site at http://irsa.ipac.caltech.edu/data/SPITZER/docs/dataanalysistools/tools/mopex/.

"check images." Background-subtracted photometry measurements were extracted for both fields using $4''$ diameter circular apertures and the appropriate corrections applied as provided in the Spitzer Science Center IRAC Instrument Handbook to scale the photometry to $24''$ apertures (to match the methodology of Ashby et al. 2009). There are 38,851 and 34,228 unique sources detected in the [3.6] and [4.5] IRAC bands in DEEP2 Fields 2 and 4, respectively.

Within the SDWFS–Boötes catalog, IRAC sources have optical counterparts that were identified within a radial distance of $\delta < 2''.5$, equivalent to a spatial distance of ~ 12.5 kiloparsecs at the median redshift ($z \sim 0.35$) of the Boötes sample. To maintain consistency, we spatially associated the IRAC sources in the DEEP2 regions to the DEEP2 photometric catalog (Coil et al. 2004) using a matching radius of $\delta = 1''.5$ (equivalent to a spatial distance of ~ 12 kpc at $z = 1$). Of the IRAC sources detected with signal to noise $\geqslant 5$ in all four IRAC bands, 3932, 1068, and 837 sources were matched to an optical spectroscopic counterpart in the DEEP2 catalog in Fields 1, 2, and 4, respectively. We tested our choice of matching radius using the IRAC–EGS data (Field 1), as the mid-IR data within this field are the most sensitive and the optical photometry is the most complete of the DEEP2 fields. We artificially shifted the positions of the IRAC sources by $1'$ to create a pseudo-random source catalog and re-performed the counterpart matching. We identify 105 fake matches, suggesting a worst-case spurious matching fraction of $\sim 2.7\%$ for the IRAC counterparts. The spurious fraction in Fields 2 and 4 are likely to be considerably smaller due to the shallow IRAC data and preselection of $z > 0.7$ targets in the optical DEEP2 spectroscopic catalog.

We identified mid-IR AGN in Boötes and DEEP2 based on their position in the typical IRAC color–color magnitude diagrams. AGN may be identified in IRAC color space when the AGN-produced power-law can be detected above the expected host-galaxy star formation emission (i.e., a sufficiently high AGN to star formation ratio). The two most widely used formalisms are the AGN selection wedges presented by Lacy et al. (2004) in $S_{8.0}/S_{4.5}$ versus $S_{5.8}/S_{3.6}$ color space and Stern et al. (2005) in [3.6]–[4.5] versus [5.8]–[8.0] color space. These AGN selection criteria were most recently updated by D12. Figures 3(b) and (c) presents the [3.6]–[4.5] versus [5.8]–[8.0] distributions (in Vega magnitudes) for all IRAC sources with Boötes and DEEP2 counterparts in our optical parent galaxy catalog (see Section 2 and the Appendix).

AGN selection in IRAC color–color space provides a relatively clean sample of AGN that is redshift-independent. However, as shown by D12, for specific redshift regimes and inherent dust extinctions, contamination from starbursting or passive systems can be significant, particularly for the Lacy criterion. In Boötes and DEEP2, we have the advantage that the IRAC sources have well constrained spectroscopic redshifts, and we may flag and remove (contaminant) sources that would be otherwise identified as AGN candidates but lie in the region of IRAC color parameter space that may be occupied by non-AGN at a given redshift.

Following D12, we track the expected positions of non-AGN galaxies in Stern color space using the SEDs of the template galaxies described in the previous section. We convolved the template SEDs with the IRAC filters to predict the position of these non-AGN systems in the Boötes and DEEP2 redshift ranges. As we show in Figures 3(b) and (c), and has been shown previously by D12 (see also Mendez et al. 2013), the lower portion of the Stern AGN wedge suffers from significant

contamination from pure starburst galaxies at $z \sim 0.5$–0.7 and $z \gtrsim 1.2$. To mitigate the contamination from starbursts to an IR AGN sample, we set a redshift-dependent threshold to the lower [3.6]–[4.5] cut that bounds the Stern AGN wedge in the Boötes and DEEP2 IR samples, as follows:

$$\text{at} \quad 0.4 < z \leqslant 0.6 : [3.6] - [4.5] > 0.2([5.8] - [8.0]) + 0.28 \tag{1}$$

$$\text{at} \quad 0.6 < z \leqslant 1 : [3.6] - [4.5] > 0.2([5.8] - [8.0]) + 0.18 \tag{2}$$

$$\text{at} \quad z > 1 : [3.6] - [4.5] > 0.2([5.8] - [8.0]) + (0.5z - 0.32), \tag{3}$$

i.e., in the redshift range $0.6 < z < 1$ a standard Stern AGN wedge may be used, as we predict it remains relatively free of contamination from star-forming systems in this redshift regime. Otherwise, in the redshift ranges where contamination is expected to the AGN sample, we flag and remove these possible star-forming interlopers. Hence, starburst systems should not enter into AGN-selected catalogs. In principle, due to the large number of star-forming galaxies that lie marginally below our imposed AGN demarcation, due to photometric uncertainties, these systems could scatter up into the AGN region. To assess this possible contamination factor, we used a Monte Carlo simulation to randomly select *Spitzer* IRAC photometric measurements based on the measured uncertainties of the IR sources in the SDWFS. Over 10,000 simulations, we found that we expect only ~ 3 ($< 2\%$) sources to be possibly spurious within the AGN region. This result is mainly driven by the small uncertainty (< 0.03 mag) on the [3.6] and [4.5] measurements, as these are the two most sensitive *Spitzer* bands. Thus, contamination from star-forming galaxies due to random measurement uncertainties is negligible.

We select IRAC AGN in Boötes and DEEP2 using both our modified, redshift-dependent Stern et al. (2005) wedge in [3.6]–[4.5] versus [5.8]–[8.0] color space or the strict (redshift independent) D12 criteria in $S_{8.0}/S_{4.5}$ versus $S_{5.8}/S_{3.6}$ color space, i.e., we consider a galaxy to contain an IR AGN if it appears in either of the AGN wedges. Our final clean IR AGN samples contains 151 and 135 sources in Boötes and DEEP2, respectively.

3.2. X-Ray AGN

Blank-field X-ray surveys arguably provide the most efficient and unbiased AGN selection, as X-ray emission is relatively unaffected by moderate levels of obscuration and remains uncontaminated by host-galaxy emission for luminosities in excess of $L_{X,0.5-7\,\text{keV}} \gtrsim 10^{42}$ erg s^{-1} (e.g., Moran et al. 1999; Lira et al. 2002). Here, we harness the unprecedented angular resolution provided by the *Chandra X-ray Observatory* to identify X-ray luminous AGN lying within the SDSS, Boötes, and DEEP2 survey regions.

The Chandra Source Catalog (CSC; Evans et al. 2010) provides a uniform catalog of high-significance X-ray sources

for all observations performed by *Chandra*. As part of the CSC analysis, a cross-matched catalog is provided between the SDSS-DR7 release and the current public release of the CSC (v1.1) using a Bayesian matching routine and contains ∼8950 extragalactic sources.[11] Despite covering ∼130 deg², the CSC–SDSS catalog cannot be considered a true blank-field survey as the majority of observations within the SDSS regions are individual pointed targets preselected for *Chandra* observations. To guard against these potentially biased *Chandra* targets, we flagged and removed all X-ray sources within 10″ of the *Chandra* aim-point. Arguably, the choice of 10″ is arbitrary. However, 10″ ensures that we remove X-ray sources that are within the expected extent of a typical galaxy at $z \sim 0.05$ (the spatial scale at $z = 0.05$ is ∼960 pc arcsec^{-1}) where we may be sensitive to contamination from stellar-mass X-ray binaries. Furthermore, our choice of 10″ allows for marginal offcenter pointings of *Chandra* and discrepancies in perceived target source position. We used the SDSS source ID numbers to directly match the remaining sources in the CSC–SDSS catalog to our matched galaxy sample and found 242 optical–X-ray sources in common when considering only those CSC–SDSS sources with a Bayesian matching probability of $P > 0.9$ in the redshift range $0.05 < z < 0.2$.

Boötes and DEEP2 have almost complete coverage by *Chandra*, and dedicated source-matched catalogs for these surveys are available (Murray et al. 2005; Kenter et al. 2005; Nandra et al. 2005; Laird et al. 2009; Kochanek et al. 2012; Goulding et al. 2012b). Here, we used the most recent cross-matched catalogs for Boötes and DEEP2 from Kochanek et al. (2012) and Goulding et al. (2012b), respectively. The X-Boötes and X-DEEP2 surveys are contiguous with ∼7.6 deg² and ∼2.7 deg² of their respective optical spectroscopic surveys with total effective X-ray exposures in the range 5 ks–1.1 Ms. When accounting for our source matching and selection process, defined in the Appendix, there are 199 and 214 galaxies with X-ray counterparts in the Boötes and DEEP2 fields, respectively.

For all of the X-ray sources in our matched catalogs, we applied X-ray K-corrections to produce rest-frame X-ray luminosities,

$$L_{\text{X,rest}}(0.5 - 7) = 4\pi d_l^2 (1 + z)^{\Gamma-2} S_{\text{X,obs}}(0.5 - 7), \quad (4)$$

where d_l is the luminosity distance and assuming a typical X-ray spectral slope of $\Gamma \sim 1.7$ (Tozzi et al. 2006). To remove possible contamination from galaxies whose X-ray emission may be dominated by high-mass X-ray binary systems and not AGN activity, we selected only sources with $L_{\text{X,rest}} \gtrsim 10^{42}$ erg s^{-1}. Our final SDSS, Boötes, and DEEP2 catalogs contain 73, 196, and 200 X-ray luminous AGN, respectively.

3.3. Radio AGN

Finally, we selected a sample of radio-luminous AGN within the three surveys. As has been shown previously, radio-loud AGN are generally identified in massive passive galaxies (e.g., Best et al. 2005; Kauffmann et al. 2008; Hickox et al. 2009). Hence, and by contrast to IR and X-ray AGN, radio-loud AGN may represent a separate AGN population and/or a different evolutionary phase of galaxy and AGN activity.

As part of the current release of the FIRST radio catalog, a matched SDSS (and Two Micron All Sky Survey) source list

is available directly from the SDSS SkyServer. For the radio objects identified to be double or triple component sources in the FIRST catalogs, we used the centroided positions. For the lowest-significance FIRST sources (the typical detection threshold is ∼0.75–1 mJy), the radio centroided positions have typical random uncertainties of <0″.5, and systematic uncertainties of <0″.05. We limited our selection to those FIRST sources within 0″.6 of an SDSS counterpart to provide a clean selection of SDSS–FIRST sources. If the FIRST radio positions are systematically offset from the optical nucleus, projection effects may adversely bias our cross-matching to only selecting counterparts at the upper-end of our redshift range. Hence, we tested the use of $\delta = 0″.6$ as compared to a larger radius of $\delta = 3″.0$, while we found a significant increase in the number of possible counterparts for the larger radius, the overall redshift distribution of the counterparts remained unchanged. Thus, our choice of matching radius can be considered clean and robust.

For the ∼6% of FIRST sources with multiple possible SDSS counterparts in the SDSS–FIRST SkyServer catalog, we chose the SDSS galaxy with the smallest separation from the FIRST source. Of these FIRST sources with multiple declared SDSS matches, each has one counterpart within <0″.6, and other (spurious) SDSS counterparts at 1″.5–8″. There are 6959 FIRST sources with SDSS counterparts within $\delta = 0″.6$ in the redshift range, $0.05 < z < 0.2$.

The Deep Westerbork 1.4 GHz radio telescope (WSRT) catalog of the Boötes field (de Vries et al. 2002) contains 3172 5σ detected unique sources down to a 1σ background limiting flux of 28 μJy. We matched all radio sources to optical counterparts within 1″.5, which accounts for the larger systematic positional uncertainty in the Westerbork imaging (median ∼0″.5) compared to the 0″.05 systematic uncertainty in the VLA FIRST data in our SDSS-matched catalog. There are 259 WSRT radio sources with spectroscopic Boötes counterparts at $0.2 < z < 0.7$.

Finally, the DEEP2 fields are covered by the FIRST VLA survey, while a dedicated deep (50 μJy) 20 cm VLA survey, AEGIS20 (Ivison et al. 2007; Willner et al. 2012) additionally covers the EGS (DEEP2 Field 1). Following our strategy for cross-matching and selection of sources between VLA and SDSS, we selected all centroided radio sources within 0″.6 of a DEEP2 optical counterpart. We found 180 radio sources in our cross-matched VLA–DEEP2 catalog at $0.7 < z < 1.4$.

Using our radio–optical cross-matched catalogs, we perform the necessary rest-frame radio K-corrections and calculate radio luminosities,

$$L_\nu(\nu_{\text{rest}}) = 4\pi d_l^2 (1 + z)^{\alpha-1} S_\nu(\nu_{\text{obs}}), \quad (5)$$

where S_ν is the FIRST radio flux at 1.4 GHz and assuming a radio spectral slope of $\alpha = 0.5$. To guard against the selection of luminous starburst systems, we selected as radio AGN only sources with $P_{1.4\,\text{GHz}} > 10^{24}$ W Hz^{-1}. Assuming a typical radio to star formation rate (SFR) conversion of log(SFR) = log($\nu L_{1.4\,\text{GHz}}$) − 37.07 (Condon 1992), the required SFR for a starburst galaxy to erroneously meet our AGN selection threshold is SFR ∼ 1200 $M_\odot$ yr^{-1}, typical of a hyper-luminous infrared galaxy. In the redshift ranges considered here, the space density of star-forming galaxies with $L_{1.4\,\text{GHz}} > 10^{24}$ W Hz^{-1} is predicted to be $\Phi \sim 6 \times 10^{-7}$ at $0.05 < z < 0.2$, ∼7 × 10^{-6} at $0.2 < z < 0.7$, and ∼10^{-5} Mpc^{-3} dex^{-1} at $0.7 < z < 1.4$ (Smolčić et al. 2009). Thus, we estimate that ∼5, ∼2, and ∼3 of the $P_{1.4\,\text{GHz}} > 10^{24}$ W Hz^{-1} radio sources identified in the SDSS, Boötes, and DEEP2, respectively, will have their

---

[11] For further information on the CSC–SDSS cross-matched catalog, see http://cxc.harvard.edu/csc1/CSC-SDSSxmatch/.
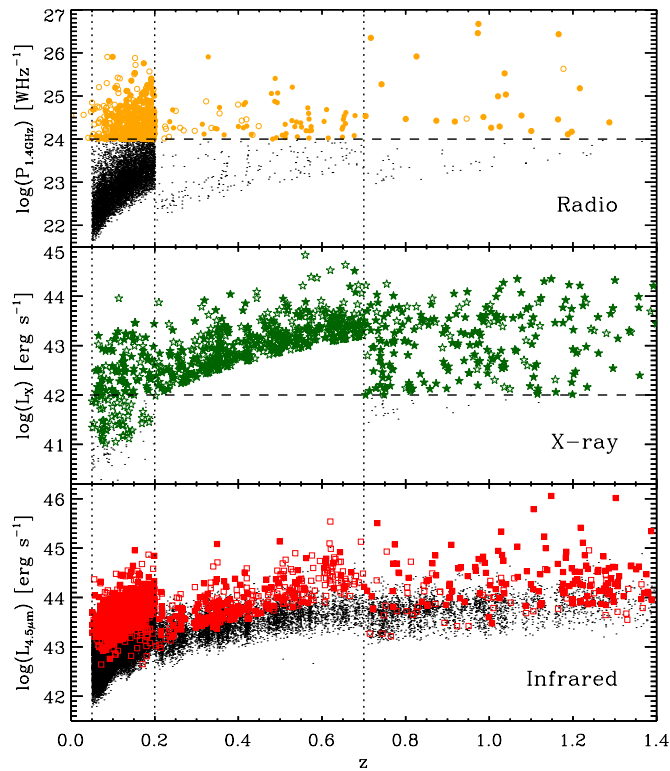
Figure 4. Luminosity distributions of galaxies (dots) and radio, X-ray, and IR AGN (filled circle; star; squares, respectively) in the survey samples. Radio AGN are selected at the threshold of $P_{1.4\,GHz} > 10^{24}$ W Hz^{-1}, and X-ray AGN with $L_X > 10^{42}$ erg s^{-1}. As part of the galaxy-matching procedure described in Section 2 and the Appendix, we remove galaxies that would hitherto not be detected in one of more of the three survey fields. For comparison purposes, those AGN hosts that are not included in the final optical-property-matched sample are shown here with open symbols.

(A color version of this figure is available in the online journal.)

radio emission dominated by rapid star formation and not AGN activity. Hence, we may consider $P_{1.4\,GHz} > 10^{24}$ W Hz^{-1} a conservative and robust choice of luminosity threshold to identify AGN. Furthermore, the relatively modest depth of the FIRST survey ($P_{limit}(z \sim 1) \approx 2 \times 10^{24}$ W Hz^{-1}) does not affect our ability to detect luminous radio-loud AGN in the DEEP2 survey as the majority ($\sim70\%$) of the radio sources identified in the DEEP2 fields have rest-frame luminosities of $P_{1.4\,GHz} \sim (0.3-4) \times 10^{24}$ W Hz^{-1}.

Our choice of radio luminosity threshold will select against moderately radio-quiet AGN, of which there are a substantial number in the SDSS (~2000; see Mullaney et al. 2013). However, our goal here is not to select a highly complete sample of radio AGN but instead one that is free from contamination from star-formation-dominated galaxies so that we may accurately compare the AGN host galaxies and their subsequent evolution. Therefore, our final conclusions toward the evolution of radio AGN are restricted to only the highest luminosity population.

The redshift distributions for the IR, X-ray, and radio AGN samples are presented in the lower panels of Figure 2 and the redshift–luminosity distributions are shown in Figure 4. In general, we span similar AGN luminosity regimes throughout the three surveys. Despite the differing sensitivities of the IRAC observations in DEEP2 Field 1 and Fields 2 and 4, it is important to consider these observations together as a combined sample because the limited survey area of Field 1 does not yield sufficient sources to cover the full luminosity range found in

Boötes and the SDSS. Finally, due to the sensitivity limit of the *Chandra* observations in Boötes, we are incomplete for AGN with $L_X \sim 10^{42}-10^{43}$ erg s^{-1} at $0.4 < z < 0.7$. In this redshift regime, we are restricted toward relatively modest to high Eddington ratio sources in low-mass galaxies, due to our ability to detect only the most luminous AGN with smaller BHs. However, this does not limit our conclusions toward the identification of the effects of AGN feedback, as it is high Eddington ratio AGN that are expected to being undergoing significant evolutionary events.

4. THE EVOLUTION OF AGN HOST GALAXIES TO $z < 1.4$

Evidence is now emerging that long-term AGN activity traces star formation in galaxies, suggesting a strong link between the properties of AGN and their host galaxies (e.g., Chen et al. 2013; Hickox et al. 2014, and references therein). Links between AGN accretion type and the evolution of their host are likely to be reflected in the host characteristics. For example, based on sensitive multiwavelength observations in the nearby universe, the most rapidly growing BHs are preferentially found in relatively low-mass, star-forming galaxies (e.g., Goulding & Alexander 2009) and are rarely found in large, passive systems (e.g., Hickox et al. 2009), supporting a paradigm whereby a substantial gas reservoir is required to simultaneously grow the BH and sustain the birth of new stars. Furthermore, at more moderate redshifts ($z \sim 1-2$), the most luminous, gas, and dust-rich starburst galaxies are commonly associated with powerful, often heavily obscured AGN (e.g., Page et al. 2004; Alexander et al. 2005).
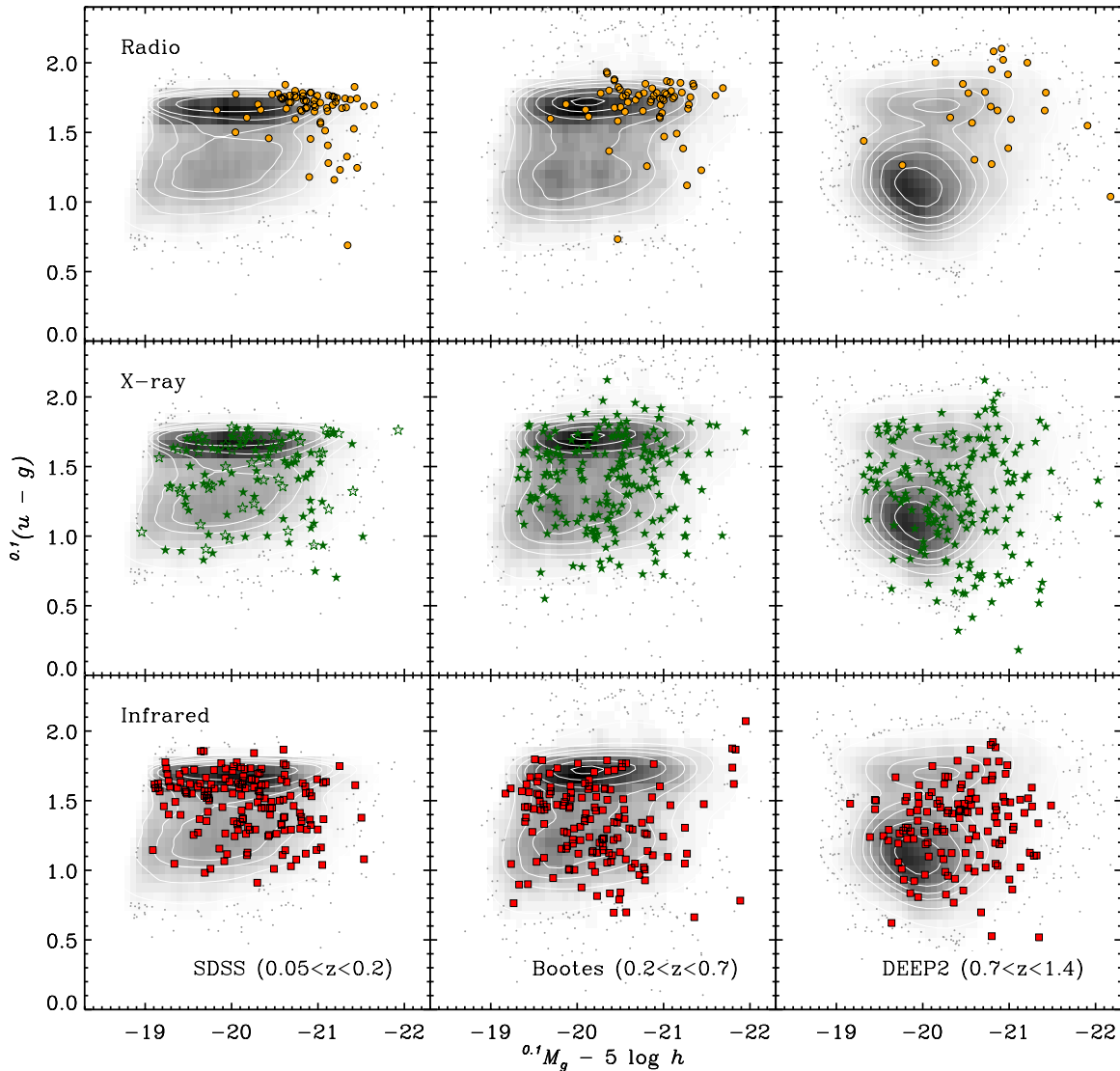
4.1. The Color–Magnitude Distribution of AGN Hosts to $z < 1.4$

A particularly powerful diagnostic for understanding the most general properties of galaxies (i.e., luminosity; mass; evolution) is their distribution in rest-frame color and absolute magnitude parameter space. The galaxy color–magnitude diagram is bimodal (e.g., Strateva et al. 2001; Hogg et al. 2003; Baldry et al. 2004; Faber et al. 2007) with a distinct separation between passive red-sequence galaxies and the blue cloud of actively star-forming systems.

To determine whether a relationship exists between galaxies that host AGN and their galaxy properties, and more importantly, to assess if such a relationship evolves with redshift, we can examine the distribution of AGN in host-galaxy color–magnitude space. Figure 5 presents the $^{0.1}(u - g)$ versus $^{0.1}M_g$ color–magnitude distributions for the galaxies in our property-matched optical catalog separated in three redshift slices, $0.05 < z < 0.2$, $0.2 < z < 0.7$, and $0.7 < z < 1.4$. Overlaid in the diagram are those sources detected as AGN in the radio, X-ray, and/or mid-IR surveys.[12]

As expected, given the strongly evolving galaxy luminosity function from $z \sim 1.5$ to the present day, combined with the bias in the original DEEP2 selection against red galaxies (Willmer et al. 2006; Faber et al. 2007 and references therein), Figure 5 shows that the galaxies identified in DEEP2 (at $0.7 < z < 1.4$) are heavily dominated by blue-cloud systems. Conversely, the SDSS galaxies (at $0.05 < z < 0.2$) are dominated by those in the red sequence, while Boötes galaxies

---

[12] For presentation purposes only, we show a random subset of the radio and IR AGN detected in the SDSS. However, for all of our cross-correlation analyses, we utilize the entire AGN ensemble.

Figure 5. Rest-frame optical color–magnitude distributions of AGN hosting galaxies at $z < 0.2$ (SDSS; left column), $0.2 < z < 0.7$ (Boötes; center column), and $0.7 < z < 1.4$ (DEEP2; right column). Photometry for the galaxy samples have been K-corrected and converted to equivalent SDSS u and g filters at $z = 0.1$, and absolute g-band magnitudes are corrected for passive evolution (e.g., Blanton et al. 2003b; Blanton & Roweis 2007). The color–magnitude diagrams for the selection-matched galaxy populations, in each redshift range, are shown with grayscale contours. Overlaid on the optical color–magnitude diagrams are radio ($P_{1.4\,\mathrm{GHz}} \gtrsim 10^{24}$ W Hz^{-1}), X-ray ($L_X \gtrsim 10^{42}$ erg s^{-1}), and IR-selected AGN which are shown with filled orange dots, green stars, and red squares, respectively. Low-redshift ($z < 0.2$) X-ray AGN identified in the SDSS (with $L_X \sim 10^{41}$–10^{42} erg s^{-1}) are shown with open green stars. From Markov Chain Monte Carlo two-dimensional Kolmogorov–Smirnov testing, we find that in each redshift regime, radio AGN are almost exclusively hosted in passive red galaxies with little evidence for evolution in their host-galaxy color–magnitude distributions. Furthermore, we find that at all redshifts X-ray AGN are spread throughout the color–magnitude diagram, with similar distributions at all redshifts, while IR AGN may show marginal evidence for evolution between $0.7 < z < 1.4$ and $0.2 < z < 0.7$.

(A color version of this figure is available in the online journal.)

are undergoing a transition due to the assembly of dense group and cluster environments, which host the majority of red-sequence galaxies in the present-day universe. Previous analysis of the color–magnitude distributions of SDSS and DEEP2 galaxies have found fundamentally similar results (e.g., Blanton 2006) in that galaxies appear intrinsically bluer at higher redshift, and these blue galaxies compose the dominant fraction of galaxies in DEEP2 (Willmer et al. 2006). By applying the evolution corrections (see the Appendix) to the red-sequence and blue-cloud galaxies of Blanton (2006), as well as the like-for-like galaxy matching between SDSS, Boötes, and DEEP2, we find similar overall color–magnitude distributions to those found previously.

The previous study of AGN within the spectroscopically identified galaxies at $0.25 < z < 0.8$ in Boötes (Hickox et al.

2009) investigated the average $^{0.1}(u - r)$ distributions of radio, X-ray, and IR AGN. They found that radio AGN are generally confined to the most massive red-sequence galaxies (see also Dunlop et al. 2003; Best et al. 2005). Furthermore, they found that while X-ray AGN are spread across a wide range in host-galaxy color (see also Xue et al. 2010; Symeonidis et al. 2013), the median color of an X-ray AGN is that of a "green-valley" galaxy (i.e., a galaxy lying between the blue cloud and red sequence; see also Nandra et al. 2007; Schawinski et al. 2007b; Coil et al. 2009; Georgakakis & Nandra 2011), and finally, they found that IR AGN are generally blue-cloud galaxies and/or less massive satellite galaxies that populate the faint end of the red sequence (but see also Mendez et al. 2013). After imposing our strict sample selection techniques to allow our comparison to SDSS and DEEP2, we obtain almost identical results to

Hickox et al. (2009) for the three AGN detection techniques. We also confirm the large range in galaxy color (∼1.6 mag) for X-ray AGN, spanning almost the entire color–magnitude diagram without evidence for a bimodal distribution as observed in the main galaxy population. Although we select only a subset of the main galaxy populations available in each survey field, it appears that, to first order, our sample is a representative subgroup that accurately reproduces previous results for both AGN (in Hickox et al. 2009) and the main SDSS–DEEP2 galaxy population (in Blanton 2006), serving as a good sanity check for our methodology.

Figure 5 further shows that in all three redshift ranges, the radio AGN are primarily confined to high-luminosity (high galaxy mass) red-sequence galaxies, while the IR and X-ray AGN are distributed throughout the color–magnitude diagram. Qualitatively, the X-ray AGN have a similar color–magnitude distribution across the SDSS, Boötes, and DEEP2 surveys, i.e., the median host-galaxy colors of X-ray AGN appear similar at all redshifts (to $z \sim 1.4$). Furthermore, the color–magnitude distributions of radio AGN appear the same at all redshifts. Such results may be in conflict with the evolving galaxy population where the blue-cloud galaxies are transitioning onto the red sequence throughout these epochs. By contrast, there is qualitative evidence that the distributions of IR AGN change between Boötes and DEEP2, with a further marginal change in the IR AGN distributions between Boötes and the SDSS.

An alternate line of investigation would be to trace the AGN host galaxies as a function of stellar mass (e.g., X-ray AGN host-galaxy properties; Aird et al. 2012), although given the limited photometric coverage of the surveys considered here, stellar-mass estimates become inherently degenerate and inaccurate in these sources. We cannot be complete to a single stellar-mass limit across the entire redshift range in either red-sequence or blue-cloud galaxies because our galaxy property corrections unphysically alter the implied stellar-mass function for these sources. However, given that our final luminosity-matched sample is designed in the SDSS rest-frame, we can use the mass-to-light conversions of Bell et al. (2003) to at least tentatively place our sample into the stellar-mass regime to allow a first-order comparison to previous investigations. Based on our limiting galaxy color and luminosities of $^{0.1}(u-g) \sim 0.60$ and 1.65 and $M_g \sim -18.9$ and -19.1 for red-sequence and blue-cloud galaxies, respectively, we estimate that at $z < 0.2$, our sample is equivalent to a stellar-mass-limited sample with $M_{*,\mathrm{blue}} \approx 8 \times 10^9 \, M_\odot$ and $M_{*,\mathrm{red}} \approx 2.6 \times 10^{10} \, M_\odot$.

4.2. Evidence for AGN Host Galaxy Evolution

We performed a two-dimensional (2D) Kolmogorov–Smirnov (K-S) test (Peacock 1983) between AGN populations at given epochs to statistically analyze their distribution in color–magnitude space and search for statistical similarities. Given the varying degree of uncertainty toward the individual optical K-corrections between the three surveys, as well as the relatively small number of sources for a given AGN type and redshift bin, we employed a 2D K-S test within a Markov Chain Monte Carlo (MCMC) routine combined with a bootstrap analysis to robustly calculate the statistical association significance between the AGN samples.

4.2.1. Constructing a Robust Two-dimensional Kolmogorov–Smirnov Test of AGN Host Distributions

For individual sources, we modeled the uncertainties in the color–magnitude measurements as 2D Gaussians with FWHM

values of $2.35\sigma_{\mathrm{i,j}}$, where σ_i and σ_j are the uncertainties on the $^{0.1}(u$–$g)$ color and absolute g-band magnitudes, respectively. These uncertainties were derived directly from the template fitting during the KCORRECT process described in the Appendix. Typically, the uncertainties on the galaxy colors are ∼0.08, ∼0.10, and ∼0.19 for sources in the SDSS, Boötes, and DEEP2 surveys, respectively. For each AGN population, selected at a given wavelength and redshift (i.e., each panel of Figure 5), we constructed 10,000 random samples from the individual source model uncertainties. We used a flat Heaviside prior to limit the random sampling to the range in color–magnitude measurements found in the main parent population distribution. To guard against outliers and false detections, which can be a particular problem during 2D K-S testing, we used a heuristic bootstrap to randomly select 90% of the detected AGN in each panel and performed a 2D K-S test between each of the panels for the 10,000 random samples drawn from the individual measurement uncertainties. More specifically, after each K-S test, we used a random-walk Metropolis–Hastings (M-H) sampler as part of the bootstrap routine to re-evaluate and adaptively weight each individual source based on its overall contribution to the K-S result. Using the 10,000 simulated measurements, the M-H sampler has the effect of minimizing the contribution of an outlier (i.e., a possible false optical counterpart) to the K-S probability. We built full probability distributions of the 9000 (10,000 × 90%) K-S test results for each of the AGN populations in the given redshift slices. We then calculate the maximum a posteriori (MAP) values for each set of AGN populations directly from the peak of the probability distributions.[13]

We tested our methodology by constructing mock samples of correlated and non-correlated data. These mock samples were built by mixing directly correlated 2D data with random "noise" in predefined proportions while maintaining overall 2D distributions that were similar to the main bimodal galaxy distribution readily observed in the three surveys. The K-S distributions from our mock catalogs were characterized by strongly skewed log-normal (almost one-sided) distributions with extended tails toward low probabilities and rapid declines from the peak of the K-S distributions (the MAP values) toward marginally larger probabilities. Mock samples consisting of 100% non-correlated data, the MAP value was invariably K-S(MAP) ≪ 0.001. For partially correlated populations (i.e., pre-determined mixtures of correlated and non-correlated data) the MAP was in the range 0.001 < K-S(MAP) < 0.02 for 67% of sample mixtures, 0.02 < K-S(MAP) < 0.2 for 95% of mixtures, and K-S(MAP) > 0.20 for 99.9% of mixtures. Hence, we can consider a positive association between two populations at the 1σ confidence level to have 0.001 < K-S(MAP) < 0.02.

4.2.2. Results of the 2D K-S Evaluation

Table 2 presents the MAP values of the K-S distributions c-alculated for the cross-association of each panel in Figure 5 (i.e., we calculate the 2D K-S MAP value for $\mathrm{AGN}_{\mathrm{SDSS,radio}}$ versus $\mathrm{AGN}_{\mathrm{Bootes,radio}}$; $\mathrm{AGN}_{\mathrm{SDSS,radio}}$ versus $\mathrm{AGN}_{\mathrm{DEEP2,radio}}$; $\mathrm{AGN}_{\mathrm{Bootes,X\text{-}ray}}$ versus $\mathrm{AGN}_{\mathrm{Bootes,IR}}$ etc.). For cross-associations which yield K-S(MAP) < 10^{-3} during our 2D K-S analysis, we instead provide the 3σ upper-limit of the K-S value (i.e., the K-S value encompassed by the lower 99.7% of the random

---

[13] The MAP values are similar in principle to a maximum likelihood value with the added stipulation of our choice of Heaviside prior to limit the distribution of color–magnitude measurements.

Table 2
Cross-correlation Analysis of AGN Host-galaxy Color–Magnitude Distributions

		SDSS $0.05 < z < 0.2$			Boötes $0.2 < z < 0.7$			DEEP2 $0.7 < z < 1.4$		
		IR	X-ray	Radio	IR	X-ray	Radio	IR	X-ray	Radio
DEEP2	Radio	<0.07	4.1×10^{-3} (<0.02)	0.29	$<10^{-3}$	3.0×10^{-3} (<0.02)	0.36	<0.07	<0.04	$\cdots$
	X-ray	1.8×10^{-3} (<0.26)	0.25	$<10^{-5}$	0.04 (<0.70)	0.12	$<10^{-5}$	0.20	$\cdots$	
	IR	1.0×10^{-3} (<0.11)	0.17	$<2 \times 10^{-5}$	0.04 (<0.78)	0.07 (<0.81)	$<10^{-5}$	$\cdots$		
Boötes	Radio	$<10^{-5}$	$<3 \times 10^{-3}$	0.30	$<10^{-5}$	$<10^{-4}$	$\cdots$			
	X-ray	0.02 (<0.58)	0.52	<0.03	0.02 (<0.50)	$\cdots$				
	IR	0.01 (<0.34)	0.10	$<10^{-5}$	$\cdots$					
SDSS	Radio	$<2 \times 10^{-3}$	<0.04	$\cdots$						
	X-ray	0.11	$\cdots$							
	IR	$\cdots$								

Notes. Maximum a posteriori (MAP) value produced from a Markov Chain Monte Carlo two-dimensional Kolmogorov–Smirnov and bootstrap analysis which calculates whether two AGN populations at a given epoch are drawn from the same parent AGN population. For cross-associations with K-S(MAP) $< 10^{-3}$, the 3σ upper limit is given and was calculated from the K-S value encompassed by the lower 99.7% of the 10,000 random samples in the 2D K-S test (red box). K-S(MAP) $\gtrsim 0.2$ indicates a high likelihood of a statistical correlation between the color–magnitude distributions of the AGN samples at the 99% confidence level or higher (green box). For cross-associations with weak/inconclusive statistical significances, we provide the K-S(MAP) and K-S(3σ) (in parentheses).

draws). Furthermore, for those cross-associations that yield a relatively ambiguous result (i.e., only partial/weak evidence for similarities in their 2D distributions in color–magnitude space) we provide both the K-S(MAP) and the 3σ upper-limit in parentheses. For example, the cross-association of the color–magnitude distributions observed for X-ray AGN identified in DEEP2 (at $0.7 < z < 1.4$) compared with the distribution for IR AGN identified in the SDSS (at $0.05 < z < 0.2$) produces K-S(MAP) $\sim 1.8 \times 10^{-3}$ and a 3σ upper-limit of K-S(3σ) < 0.26.

The results presented in Table 2 confirm our earlier impression that at any given redshift, the host galaxies of radio AGN appear to be drawn from the same parent population, which maintains very similar color–magnitude distributions with a statisti-

cal significance of $P > 95\%$. Concurrently, the host galaxies of X-ray AGN also appear to maintain similar distributions across the redshifts, and these are not correlated with the host galaxies of radio AGN. Hence, we find strong statistical evidence that the color–magnitude distributions of AGN host galaxies have not evolved significantly in the last 9 Gyr of Cosmic history. Furthermore, as already noted by Hickox et al. (2009), the radio and IR AGN populations appear anti-correlated in Boötes galaxies. From our statistical analysis, a similar result appears to hold across all of the redshift regimes considered here; at any given redshift, IR and radio-selected AGN exist in separate host-galaxy populations. Such a result is consistent with the notion that the accretion processes are distinctly different between the X-ray/IR AGN population and the majority of the radio AGN
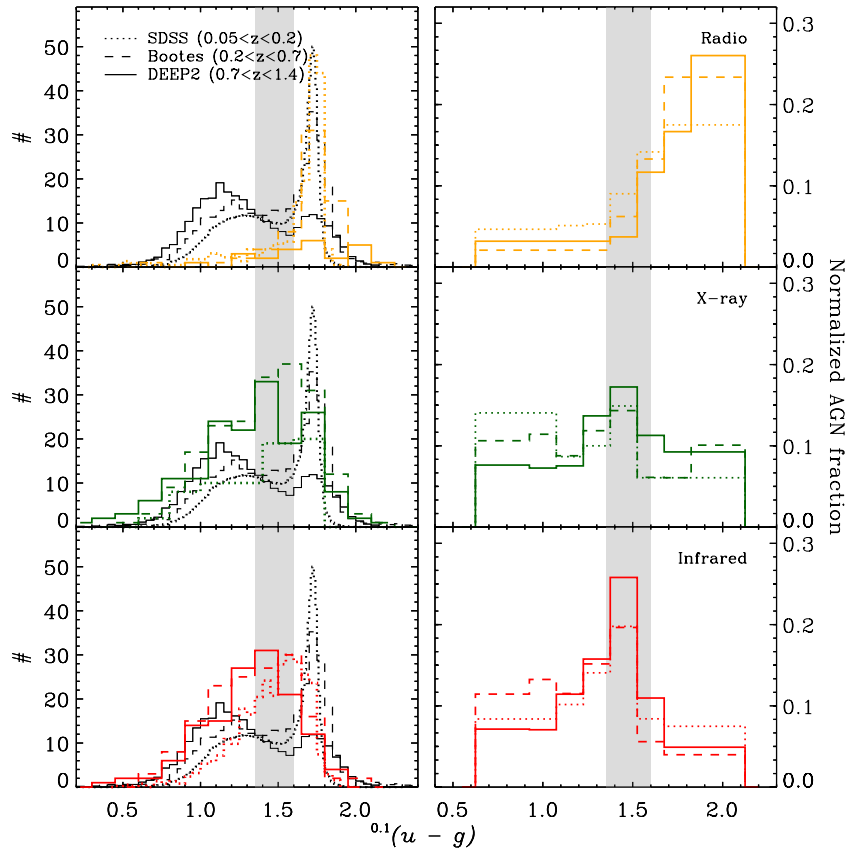
Figure 6. Left: rest-frame $^{0.1}(u - g)$ color distributions, shifted to $z = 0.1$ of radio (top panel; yellow), X-ray (middle panel; green), and IR (bottom panel; red) AGN. The respective parent galaxy populations in the SDSS ($0.05 < z < 0.2$; dotted line), Boötes ($0.2 < z < 0.7$; dashed line), and DEEP2 ($0.7 < z < 1.4$; solid line) surveys are shown in black, with the peak values scaled by a factor of 1/40 to match the AGN populations. The approximate position of the "green-valley" is shown in the shaded region. Right: same as left panel with AGN histograms normalized to the respective parent galaxy populations. AGN dominated by mechanical energy output are invariably hosted in red massive systems, and are anti-correlated with the hosts of radiatively efficient IR AGN; i.e., IR AGN are hosted in star-forming blue galaxies. When normalized for the underlying parent populations, we find little or no evidence for evolution in the host-galaxy color distributions within the last 9 Gyr. (A color version of this figure is available in the online journal.)

population. As the evolution of galaxies is expected to be a long-term process, and the host galaxies of radiatively efficient and inefficient AGN appear to be separate at a given redshift, we find little evidence for a "flip-flop" between accretion modes within the same galaxies. The original DEEP2 galaxy rest-frame UV selection and spectroscopic selection results in a marginal bias toward the selection of blue galaxies, particularly at $z > 1.1$ (see the Appendix and Faber et al. 2007). Thus, to reconcile the observed anti-correlation between IR and radio AGN, red galaxies hosting IR AGN (and not radio-loud AGN) would need to be systematically missed throughout the overall population. On the other hand, IR AGN generally present strong AGN emission lines at optical wavelengths, which would provide a bias toward their detection and inclusion in the sample. Hence, despite the deficit in DEEP2 red galaxies, it appears that the observed anti-correlation between the AGN populations is relatively robust.

The lack of a 2D correlation between IR and radio sources may only hold for low-excitation (LEX) radio AGN ($P_{1.4\,\mathrm{GHz}} \sim 10^{24}$–$10^{25}$ W Hz^{-1}). Those radio AGN in a high-excitation mode (HEX; with $P_{1.4\,\mathrm{GHz}} > 10^{25}$ W Hz^{-1}) appear to be confined to bluer galaxies ($u - g \sim 1.3$) than the LEX radio AGN (e.g., Smolčić 2009) and have (qualitatively) similar host-galaxy distributions to the X-ray and IR AGN. However, given the low-number (13) of HEX radio AGN present in Boötes and DEEP2, we lack the source statistics to place robust constraints on any

correlation on the evolution of HEX radio sources and X-ray/IR AGN.

DEEP2 reveals a substantial number of IR (35) and X-ray (39) AGN in luminous red-sequence galaxies at $z \sim 1$ that are absent at $z < 0.7$. Analysis of the luminosity distributions of these particular DEEP2 AGN finds that the galaxies are relatively high-luminosity systems with $L_{4.5\,\mu\mathrm{m}} > 5 \times 10^{44}$ erg s^{-1}. Their absence in SDSS and Boötes may be a luminosity down-sizing effect as only two (three) AGN with similar luminosities are present in the SDSS (Boötes) samples. Conversely, there is a population of IR AGN in low-luminosity ($^{0.1}M_g > -20$) red-sequence galaxies at $z < 0.7$ that do not appear at higher redshifts in DEEP2. However, we detect a small coincident population of 18 low X-ray luminosity ($L_X \sim 2$–4×10^{42} erg s^{-1}) AGN in the sensitive DEEP2 X-ray data that have similar host galaxies to those expected for the undetected IR AGN. Indeed, IR AGN identified at lower redshift have relatively low IR luminosities ($L_{4.5\,\mu\mathrm{m}} < 3 \times 10^{43}$ erg s^{-1}), which is, in general, below our sensitivity limit for IR AGN in DEEP2. In turn, this may cause the factor of $\sim$2 deficit found between red-sequence DEEP2 X-ray and IR AGN observed in the normalized populations (presented in Figure 6; see below).

Due to the relatively shallow nature ($\sim$5 ks exposures) of the current X-ray survey in the Boötes field, we are insensitive toward AGN with $L_X < 10^{43}$ erg s^{-1} at $z > 0.6$. To assess any luminosity bias that may affect these results, we split the

Boötes X-ray AGN between those sources with $L_X > 10^{43}$ and $< 10^{43}$ erg s^{-1} and reperformed our 2D K-S analysis. When considering only those X-ray AGN in the Boötes sample with $L_X > 10^{43}$ erg s^{-1}, we find a marginal change in the AGN distribution in color–magnitude space. Specifically, we find a small systematic reduction of X-ray AGN in blue-cloud galaxies with $^{0.1}M_g < -20.5$ mag. This results in a significant increase in the 2D K-S correlation between the Boötes X-ray AGN and both the SDSS X-ray (K-S(MAP) ~ 0.84) and IR AGN (K-S(MAP) ~ 0.49). In the SDSS sample, the average X-ray luminosity is a factor ~ 4 lower than our assumed 10^{43} erg s^{-1} completeness threshold in Boötes. However, we calculate that the distribution of X-ray AGN in color–magnitude space remains statistically identical between the two redshift regimes. Hence, this may be interpreted as direct evidence for luminosity downsizing within the X-ray AGN for the same galaxy population. When we conversely consider only those X-ray AGN with $L_X < 10^{43}$ erg s^{-1} in Boötes (which we limit to $z < 0.5$), we find a systematic reduction of X-ray AGN in the most luminous red galaxies. Subsequent 2D K-S testing for these lower luminosity X-ray AGN reveals statistically indistinguishable color–magnitude distributions between X-ray and IR AGN in Boötes (K-S(MAP) ~ 0.31). As we note in Section 3.1, the selection of IR AGN results in a relatively extinction-independent sample. Given that we find systematically lower (observed) X-ray luminosity AGN reside within similar galaxy populations at fixed redshift, this may tentatively suggest that more highly obscured AGN occur within the dust/gas-rich blue-cloud population. Indeed, in-depth studies of very nearby AGN find a high-incidence of obscured AGN in low-mass late-type strongly star-forming galaxies (e.g., Goulding & Alexander 2009).

Table 2 further shows that the cross-association between radio AGN and X-ray/IR AGN consistently results in K-S(MAP) < 0.01, suggesting there is little or no link between the host galaxies of luminous radio AGN and luminous X-ray/IR AGN. However, given that red galaxies were marginally biased against the original DEEP2 selection, this may be a selection effect brought about by the distribution of the underlying galaxy population. Figure 6 shows the rest-frame host-galaxy color distributions for the three AGN selection wavebands. When calculated as a fraction of the underlying galaxy population in each survey, we confirm our K-S test results that after removing the effect of the evolving galaxy population, the host galaxies of radio AGN compared to IR/X-ray AGN are anti-correlated at all redshifts, and this does not appear to be an effect of the changing galaxy population. To reduce small number statistical effects here, we use a bootstrap analysis to randomly select AGN and galaxies from the main populations. The area under the distributions are normalized to unity to allow a better comparison between the AGN types and redshift regimes.

Figure 6 shows an overdensity of IR AGN at $^{0.1}(u - g) \sim 1.5$ throughout the three surveys, similar to that seen for X-ray AGN in previous surveys (see Section 4.1), which we marginally observe for X-ray AGN here also. Such a peak in color is consistent with the expected position of the "green-valley" (e.g., Nandra et al. 2007; Schawinski et al. 2007a) in the color–magnitude diagram. There is also a factor ~ 2 increase in the fraction of radiatively efficient AGN observed in blue-cloud galaxies over red-sequence sources, suggesting that radiatively efficient AGN may, in general, be confined to blue-cloud galaxies. Physically, this can be interpreted as the AGN and star formation being fueled by similar mechanisms. This is unlikely

to be ubiquitous as a population of X-ray (and IR) luminous AGN are found in low-luminosity red-sequence galaxies. It has been previously suggested that the effect of host-galaxy dust-extinction may drive the identification of the green-valley as an evolutionary staging ground for galaxies evolving onto the red sequence (e.g., Cardamone et al. 2010; Bongiorno et al. 2012). Here, we show that the peak in the IR AGN population, combined with only a small fraction of IR AGN existing in red-sequence galaxies, may provide additional evidence that IR AGN are hosted in more obscured galaxies and are not necessarily evolving directly from blue-cloud disk-dominated galaxies into more passive elliptical systems.

When these results are taken together, after accounting for random uncertainties and the changing underlying galaxy population, the color–magnitude distribution of radio AGN host galaxies has remained similar at all times in the last 9 Gyr. While the distribution in color and luminosity is substantially larger for X-ray and IR AGN, there still appears to be little or no significant change in these distributions within the epoch considered here. Put simply, we find little evidence to suggest that the general host-galaxy properties of radio, X-ray, and IR AGN have changed or evolved in the last 9 Gyr (i.e., the host-galaxy distribution for $\{AGN_k\}_{R;X;IR}$ is almost identical at each redshift slice).

There is now an emerging picture that points toward a distinct lack of evolution in AGN hosts. At least in the X-ray AGN population, the absence of significant evolution may even hold to $z \sim 3$ (e.g., Rosario et al. 2013). Furthermore, Aird et al. (2012) recently investigated the color–stellar-mass distribution of X-ray-detected AGN using *XMM-Newton* and *Chandra* in the PRIMUS survey fields (Coil et al. 2011), and found that while they observed evolution in the specific fraction of galaxies that host AGN as a function of redshift,[14] the distribution and color dependence of the stellar-mass-independent AGN Eddington ratios (i.e., $\lambda_{Edd} \propto L_X/M_*$) have remained consistent since $z \sim 1$. Indeed, the similar distributions of X-ray AGN as a function of color and Eddington ratio found by Aird et al. (2012) may provide further evidence that the AGN triggering mechanism and fueling source are the same for radiatively efficient AGN. While a direct comparison to the previous investigation is not possible due to the limited coverage of the photometry in Boötes and DEEP2, which limits our ability to place strong constraints on the stellar masses of individual galaxies, we still find consistent and analogous results with galaxy luminosity as an indirect proxy for the stellar mass. By including the more sensitive and complete multiwavelength data, we have extended the previous results of Aird et al. (2012) to the lower Eddington radio AGN population and to $z \sim 1.4$ for X-ray and IR-selected AGN, still finding no evolution in the overall AGN population.

4.3. Similar Host-galaxy Evolution of Low-luminosity X-Ray AGN

Unfortunately, source statistics are relatively poor for the X-ray AGN identified in the SDSS. This is driven somewhat by the lack of a dedicated homogeneous *Chandra* X-ray survey

---

[14] Due to incompleteness effects, here we specifically do not investigate the absolute fraction of AGN in particular galaxy populations. For our large, non-contiguous galaxy sample, such an investigation requires a full statistical treatment of the individual sensitivities across each multiwavelength band performed on a source-by-source basis (e.g., see Aird et al. 2012 for an X-ray–optical sensitivity comparison). Hence, such an investigation is beyond the current scope of these analyses.

across the entire SDSS region as well as the significant decrease in the average AGN luminosity in the nearby universe (i.e., AGN cosmic downsizing; e.g., Ueda et al. 2003; Barger et al. 2005; Hasinger et al. 2005). Furthermore, due to the negative K-correction at X-ray energies, *Chandra* observations at low redshift are more susceptible to nuclear extinction than sources observed at higher redshift. Many galaxies with single X-ray point sources coincident with the optical galaxy nucleus may contain low-luminosity or obscured AGN.

Figure 5 additionally shows the color–magnitude distribution of the 47 X-ray-detected sources in the SDSS-DR7 with $L_X \sim 10^{41}$–10^{42} erg s^{-1}, which also meet our parent-galaxy selection methodology, outlined in the Appendix. This lower X-ray luminosity AGN population has the same host-galaxy color–magnitude distribution as their more luminous counterparts. Using the previous investigations of SDSS galaxies/AGN, which analyzed local stellar and BH mass distributions (e.g., Heckman et al. 2004; Kauffmann & Heckman 2009), and given the similar distribution of host galaxies, it is likely that these AGN are low-luminosity and/or intrinsically obscured AGN. Hence, this population of $L_X \sim 10^{41}$–10^{42} erg s^{-1} X-ray sources further reinforces our observation of the similar host-galaxy color–magnitude distributions of X-ray sources across the entire redshift range.[15]

There appears to be little systematic distinction in color–magnitude space between the general galaxy population and either the low or high X-ray luminosity AGN (i.e., X-ray AGN exist in all host-galaxy types). Such a lack of distinction between those galaxies that do and do not host a radiatively efficient AGN may suggest that at some point in cosmic time, the vast majority of galaxies have hosted an actively growing BH, and this is independent of the galaxy's individual merger history, luminosity, stellar mass, or stellar population. Whether a particular galaxy is observed to be growing the central BH at a given luminosity is likely due to intrinsic stochasticity of the accretion disk or variability of the obscuring medium surrounding the central source (e.g., Lutz et al. 2010; Aird et al. 2012; Rosario et al. 2013; Shao et al. 2013; Hickox et al. 2014).

4.4. AGN in Dense Groups and Cluster Environments

Galaxy populations in groups and clusters often differ in properties from the field population. Galaxies in groups often consist of massive spheroids hosting relatively old stellar populations, and these galaxies likely occupy the high luminosity end of the red sequence. Figures 5 and 6 show that at all redshifts, luminous radio AGN with $P_{1.4\,\mathrm{GHz}} \gtrsim 10^{24}$ W Hz^{-1} are tightly correlated with massive/luminous host galaxies that lack strong ongoing star formation signatures, i.e., they have similar properties to those in dense group environments.

A substantial fraction of the red-sequence build-up is expected to occur between $0.2 < z < 1.4$ (e.g., Bell et al. 2004; Cooper et al. 2006; Faber et al. 2007; Moustakas et al. 2013). Using the available group catalogs for both Boötes (B. Vajgel et al., in preparation) and DEEP2 (Gerke et al. 2012), we can directly compare the environmental properties of the AGN observed at or between these epochs. Both the Boötes and DEEP2 group catalogs were constructed using similar Voronoi–Delaunay methods. We identified the AGN hosted in red-sequence galaxies in

both surveys and compared these to the respective group catalogs. We found consistent fractions of $\sim$26% and $\sim$28% IR and X-ray AGN with red-sequence hosts are group members, and these fractions remain constant between $0.2 < z < 0.7$ and $0.7 < z < 1.4$ with no significant evidence for evolution. Using the known positions of the group barycenters, we assessed whether these AGN were also coincident (within 2 Mpc) of the group center. In general, these are not at the position of or even the galaxy closest to the barycenter. By contrast, we find a suggestion of an increase in the fraction of radio AGN in groups between Boötes and DEEP2. In DEEP2, at $0.7 < z < 1.4$, only $\sim$19 $\pm$ 10% (3/16) of the radio AGN are group members, consistent with the fraction found for X-ray and IR AGN in DEEP2; while $\sim$40 $\pm$ 9% (19/48) of radio AGN are in groups by $0.2 < z < 0.7$ in Boötes, and these AGN are predominantly consistent with the group center. These results suggest the location/environment of the (central) galaxy within the group may drive the production of the radio jet.

At $z \sim 1$, group/cluster environments are relatively rare and have not yet become fully established with warm/hot gas halos. Hence, at $z \sim 1$, we observe only a small fraction ($\sim$20%) of radio galaxies in group environments. The remaining DEEP2 radio galaxies are additionally IR and X-ray-detected sources; these are more likely linked with HEX radio activity. By contrast, at $z \sim 0.5$, the group environments are in place. The warm intracluster gas inhibits efficient accretion, creating powerful radio jets. These radio jets and subsequent radio lobes have the effect of preventing further cooling of the group gas, and restrict the production of new stars. This picture can be further substantiated as only two of the 13 radio galaxies present in groups at $0.2 < z < 0.7$ are also identified as AGN at X-ray and IR wavelengths. Furthermore, it appears that radio galaxies follow the build-up of group environments in red-sequence galaxies. It is then the existence of the powerful radio lobes, which are injecting mechanical energy back into the group/cluster, that prevents efficient gas cooling and restricts star formation, sustaining the radio AGN host galaxy as a red-sequence system (so-called maintenance-mode feedback; Best et al. 2005; Rafferty et al. 2006; McNamara & Nulsen 2007; Kauffmann et al. 2008; Jones et al. 2010; Bower et al. 2012.

5. DISCUSSION

Observational studies of low- and high-redshift radio galaxies have found evidence for large-scale mechanically driven outflows in the form of (often) megaparsec-scale relativistic radio jets (and associated lobes) originating from the AGN. Given that such radio jets are almost exclusively observed in central massive "red and dead" systems (e.g., Best et al. 2005; Wake et al. 2008; Hickox et al. 2009), it has been suggested that a quenching phase that transitions galaxies from having large cool gas reservoirs to being dominated by virialized hot atmospheres may be essential for the build-up of the red sequence of galaxies (Cooper et al. 2006; Bower et al. 2006, 2008; Croton et al. 2006).

In light of this, the current consensus is that galaxies likely begin as star-forming systems and become relatively passive once their dark matter halos reach sufficient mass and/or they undergo freefall into a second large halo, i.e., they experience tidal-stripping due to interaction with a group or cluster. We have found that powerful radio galaxies tend to be found in dense gas-rich environments located near the group barycenter and this appears to be true at all redshifts (to $z < 1.4$). These radio AGN are likely providing the heating source, through maintenance-mode

---

[15] To preserve our *clean* AGN selection, we do not include the $L_X \sim 10^{41}$–10^{42} erg s^{-1} AGN population for any subsequent analyses, as the X-ray emission from a subset of these low-luminosity sources may still be dominated by stellar processes and X-ray binaries.

feedback, to have a profound effect on the gas present in the host galaxy and by extension, the gas within the dark matter halo. This AGN feedback is inhibiting subsequent gas cooling and the rapid production of new stars. Indeed, as the fraction of galaxies hosting radio sources is a strong function of both BH and stellar mass (e.g., Best et al. 2005), it would appear that powerful radio sources closely follow the build-up of the most massive and luminous systems on the red sequence.

By contrast to the radio AGN population, recent large-scale galaxy population studies, focusing on the coincident presence of rapid star formation activity and radiatively efficient AGN recognized as X-ray and/or IR luminous central sources, have revealed contradictory results. In spite of the strong belief that mergers and the presence of an AGN play a significant role in quenching the ongoing star formation and transitioning galaxies from the blue cloud to the red sequence, many recent studies now suggest that X-ray/IR luminous AGN have not played a substantial role in the build-up of the red sequence. The preferred picture is secular galaxy evolution (e.g., Kocevski et al. 2012; Schawinski et al. 2012). However, even for a galaxy that is evolving through secular processes, the presence of a rapidly growing BH still necessitates a large cool gas supply to fuel accretion. When combined with a correlation between high-accretion rate AGN and star formation (e.g., Lutz et al. 2008; Bonfield et al. 2011; Juneau et al. 2013), this has led to the hypothesis that these two processes may be fueled from the same gas reservoirs (e.g., Chen et al. 2013; Hickox et al. 2014). As part of our K-S evaluation (see Section 4.2) of AGN populations at $0.05 < z < 1.4$, we found that the bulk of the radiatively efficient (X-ray; IR-detected) AGN are in predominantly star-forming (blue-cloud) galaxies. Taken together, these results provide evidence for a broad relationship between the coincident presence of an AGN and ongoing star formation. In turn, this may lead to a form of self-regulation for the growth of the central BH. We also find that any trends with redshift observed for the galaxy color, and by extension the integrated star formation of the host, appear to be similar for galaxies hosting and not hosting AGN, suggesting that while the AGN and ongoing star formation may be coincident and fueled simultaneously, the instantaneous presence of the radiatively efficient (X-ray- or IR-detected) AGN is having little effect on the evolution of the host galaxy in the last 9 Gyr. Furthermore, and as we noted previously, there is also a population of AGN present in weakly star-forming or post-starburst systems (see also Symeonidis et al. 2013). Taken together, it therefore appears that AGN and galaxy evolution may follow similar paths at all redshifts (see Figure 6).

Figure 7 presents a schematic diagram to represent the galaxy colors/types which host AGN throughout the last 9 Gyr of cosmic time. At all redshifts, mechanically dominated (LEX) radio AGN are hosted in a separate galaxy population from the radiatively efficient X-ray/IR AGN. This can be understood by powerful radio galaxies requiring a massive host with a large BH, an old stellar population, and possibly located near the center of a large group or cluster environment. By contrast, the radiatively efficient IR and X-ray AGN are generally (>80%) hosted in lower mass galaxies hosting smaller BHs with ample cool gas to fuel higher accretion. Those AGN hosted in galaxies with redder blue-cloud colors are likely to be dust rich and/or have smaller reservoirs of cool gas to fuel young star formation and the central BH.

Finally, the typical star formation gas depletion timescale (i.e., the time taken to convert the available cool gas supply into stars) is of the order several gigayears for an individual massive spiral
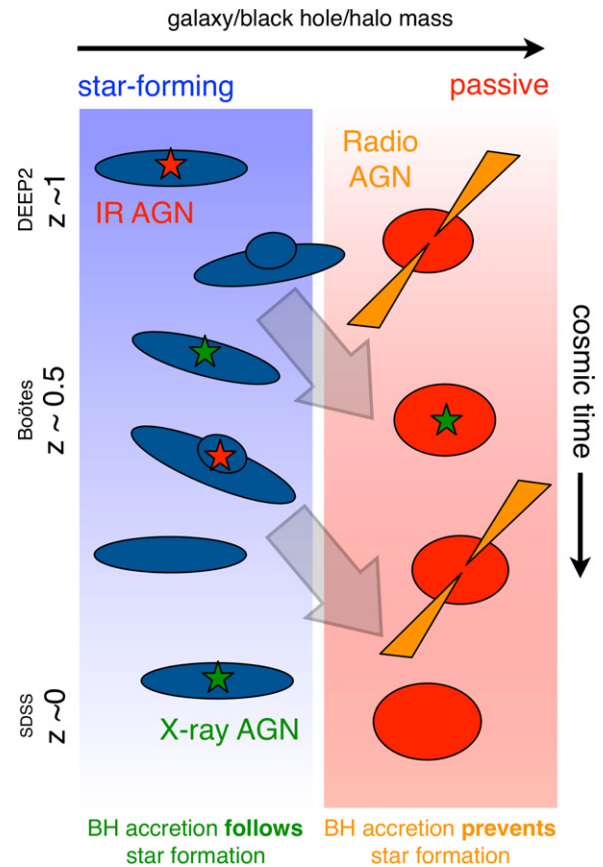
Figure 7. Schematic diagram of the evolution of AGN host galaxies throughout the last 9 Gyr of Cosmic time. From the results presented here, we find that galaxy evolution follows an apparently similar path at all redshifts. All galaxies appear to begin as star-forming blue-cloud systems and end as passive red-sequence sources, once their dark matter halos have grown sufficiently. However, we show that those galaxies hosting IR, X-ray, and/or radio AGN appear to follow a similar evolutionary path: radiatively efficient rapid BH growth (IR/X-ray AGN) appears to be linked with those galaxies with large supplies of cool gas, while mechanically dominated (radio) accretion is associated with passive galaxies, which may also be responsible for preventing late star formation.

(A color version of this figure is available in the online journal.)

galaxy. Combining this with the strong build-up of intermediate mass galaxies on the red sequence since $z \sim 1$ (e.g., Faber et al. 2007; Moustakas et al. 2013), passive evolution alone is not sufficient to explain the rapid change in the galaxy luminosity and mass function in the last 7 Gyr (e.g., Marchesini et al. 2009). The disruption to the host-galaxy gas, preventing late star formation activity, has long since been attributed to the presence of a central AGN as the required quenching mechanism. Hence, the lack of evidence for evolution in the host-galaxy colors of the radiatively efficient, X-ray and IR AGN presents a problem for the requirement of the rapid build-up of red-sequence galaxies. This likely presents two evolutionary paths. (1) The presence of an AGN has little or no impact on the evolution of galaxies, and a different mechanism is quenching the star formation in field galaxies (e.g., increased supernovae activity; self-suppression through starburst winds); or (2) the stochastic presence of a variable (and at times extremely luminous) AGN has a short-lived but significant effect on the host properties (e.g., Schawinski et al. 2010; Novak et al. 2011; Sarajedini et al. 2011; Gabor & Bournaud 2013). Such an event would be similar to a spectacular quasar-phase of galaxy evolution. Such sources are outside our sample because we require accurate measurements

of the host galaxy, which is outshone when in the presence of a quasar.

6. SUMMARY AND CONCLUSIONS

We have presented a statistical analysis of the host-galaxy rest-frame colors and luminosities of AGN at $0 < z < 1.4$ that were identified at radio, X-ray, and IR wavelengths within the SDSS, Boötes, and DEEP2 surveys. Using the available galaxy catalogs within the these three fields, we constructed a parent sample of 330,811 galaxies that are matched for luminosity and galaxy color, and corrected for passive evolution to allow a direct comparison of the sources identified throughout the $0 < z < 1.4$ epoch. We used the available multiwavelength ancillary data from *WISE*, *Spitzer*-IRAC, *Chandra*-ACIS Westerbork radio, and VLA to identify those galaxies hosting radio, X-ray, and IR AGN. Using this large multiwavelength homogeneous galaxy sample, we presented the color–magnitude distributions for the main galaxy sample and the AGN host galaxies. Through an MCMC 2D K-S analysis, we found that at all redshifts, radio AGN with $P_{1.4\,\mathrm{GHz}} > 10^{24}$ WHz^{-1}, powered by advection-dominated accretion mechanisms, are systematically hosted in luminous red-sequence galaxies. Conversely, and in line with previous studies, X-ray (with $L_X > 10^{42}$ erg s^{-1}) and IR AGN (selected through IR color–color techniques), which are undergoing radiatively efficient accretion are, in general, hosted in a separate population of blue-cloud galaxies and lower luminosity red galaxies. Despite the build up of the red sequence of galaxies throughout the epoch considered here, we find little or no statistical evidence that those galaxies that are actively growing their central BHs have evolved separately from the galaxies not hosting AGN. However, once a galaxy has become established on the red sequence, the coincident presence of a central radio source may inhibit subsequent star formation in these systems and prevent them from returning to the blue cloud. Hence, based on the statistical analyses presented here, AGN hosts appear to follow similar evolutionary paths to the main galaxy population at all times in the last 9 Gyr.

Facilities: CXO (ACIS), *Spitzer* (IRAC), *WISE*

APPENDIX

GALAXY SAMPLE DESCRIPTION AND SELECTION

In this appendix, we present an outline of the survey fields from which our main galaxy sample is selected and the composition of the multiwavelength ancillary data present within the fields. Furthermore, we include an in-depth description of the like-for-like galaxy matching procedure between the three surveys and redshift slices, along with the appropriate optical *K*-correction procedure to calculate rest-frame colors and galaxy luminosities.

A.1. The Sloan Digital Sky Survey

Our sample of relatively low-redshift galaxies, presented here, is selected from the seventh data release of the Sloan Digital Sky Survey (SDSS-DR7; Abazajian et al. 2009). The SDSS-DR7 is currently the largest publicly available optical extragalactic spectroscopic catalogue ($\approx$8032 deg^2) containing $\sim$900,000 spectroscopic galaxy redshifts. The sources are primarily identified in the northern Galactic sky with photometry determined from five-band $ugriz$ filters at $\lambda \sim$ 3550–8900 Å. The spectroscopic catalog is complete to $r < 17.77$ mag. Full optical data products are available directly from the SDSS archive, but to ensure the accuracy of the emission line identifications and photometric measurements, here we adopt the dedicated reprocessed data products from the MPA-JHU DR7 catalog (e.g., Brinchmann et al. 2004; Kauffmann et al. 2003b; Tremonti et al. 2004; LaMassa et al. 2013). The MPA-JHU catalog contains photometric and spectral measurements for $\sim$800,000 unique galaxies. For our purposes, we select the 592,300 spectroscopically targeted galaxies in the redshift range $z \sim$ 0.05–0.2.

With the advent of all-sky surveys and homogeneous data reduction systems, large moderate-sensitivity multiwavelength observations do now exist which cover substantial fractions of the SDSS sky region. At radio wavelengths, with $\sim$950,000 sources detected down to 1 mJy, the Very-Large-Array Faint Images of the Radio Sky at Twenty-Centimeters (hereafter, VLA-FIRST; Becker et al. 1994, 1995) survey covers $\sim$10,600 deg^2 of the sky, with $\sim$94% coverage of the SDSS region. At mid-infrared (mid-IR) wavelengths, we adopt the all-sky catalog of the *Wide-field Infrared Survey Explorer* (hereafter *WISE*) to provide moderate spatial resolution four-band IR photometry for the sources identified across the SDSS region (Wright et al. 2010). We describe our source-matching procedure between *WISE* and SDSS as well as our AGN identification technique in Section 3.1. While dedicated *Chandra* X-ray surveys exist for both the Boötes and DEEP2 regions, a complete *Chandra* survey of the full SDSS region is prohibitively expensive. However, archival *Chandra* data already exist for $\sim$130 deg^2 (after accounting for overlapping observation regions) between SDSS and *Chandra* as part of the Chandra Source Catalog. After removal of target *Chandra* sources, this provides a representative sample of SDSS sources with sensitive X-ray observations that are comparable to the Boötes and DEEP2 surveys.

A.2. The NDWFS Boötes Field

With $\sim$41,000 identified galaxies, primarily at $z \sim$ 0.2–0.7, the 9.3 deg^2 NOAO Deep Wide-Field Survey (NDWFS; Jannuzi & Dey 1999) Boötes field with homogeneous spectroscopic coverage from the AGN and Galaxy Evolution Survey (AGES; Kochanek et al. 2012) provides an ideal survey area to probe the moderate redshift regime. The Boötes field (R.A. = $14^{\mathrm{h}}32^{\mathrm{m}}00^{\mathrm{s}}$,

decl. $= 31^d 16^m 47^s$ [J2000]) lies at both high galactic and ecliptic latitude, and hence, is relatively free of significant foreground contamination. Optical photometry for the full NDWFS Boötes field was conducted with the 4m Mayall Telescope at the Kitt Peak National Observatory in B_W, R and I filters with z-band photometry for $\sim 62\%$ of the survey. The AGES redshift survey is complete to $I < 20.5$ mag, with redshifts determined from MMTO Hectospec observations (Fabricant et al. 2005), with $R \sim 1000$ in the wavelength range $4500 < \lambda < 8900$ Å, and covers ~ 7.74 deg^2 of the NDWFS Boötes area. Furthermore, contiguous multiwavelength observations in the mid-infrared (*Spitzer*-IRAC and MIPS; Eisenhardt et al. 2004; Stern et al. 2005; Ashby et al. 2009), far-infrared (*Herschel*-PACS and SPIRE), radio (Westerbork 1.4 GHz; de Vries et al. 2002), and shallow X-ray (*Chandra*-ACIS; Murray et al. 2005; Kenter et al. 2005; Brand et al. 2006) exist across the AGES region.

A.3. The DEEP2 Galaxy Redshift Survey

The 3.6 deg^2 DEEP2 Galaxy Redshift Survey (Davis et al. 2003; Newman et al. 2013) is currently the widest area deep spectroscopic survey of $z \sim 1$ galaxies, making it an ideal survey to target large numbers of AGN to $z \sim 1.4$. The photometric catalog for DEEP2 (Coil et al. 2004) is derived from Canada–France–Hawaii Telescope images from the 12×8k mosaic camera (Cuillandre et al. 2001) in B, R, and I filters across four non-contiguous (~ 0.6–0.9 deg^2) sky regions and is complete to $R < 25.2$ mag. The fourth data release of the spectroscopic survey contains the spectra for $\sim 50,300$ galaxies (Newman et al. 2013; with $R_{AB} < 24.1$). These galaxies are primarily in the redshift range $z \sim 0.7$–1.4 with spectroscopic redshifts determined from data collected using the DEIMOS spectrograph ($R \sim 5000$ in the wavelength range $6400 < \lambda < 9200$ Å) on the Keck II telescope. All four DEEP2 fields have X-ray coverage using the *Chandra* X-ray Telescope (the XDEEP2 survey; Goulding et al. 2012b) with combined exposures in the range ~ 10–800 ks. Field 1 of DEEP2 has dedicated VLA radio (Ivison et al. 2007; Willner et al. 2012) and *Spitzer* mid-IR photometry (Barmby et al. 2008) as part of the All-wavelength Extended Groth Strip International Survey (AEGIS; see Davis et al. 2007 for an overview). DEEP2 Fields 2 and 4 have sensitive *Spitzer* mid-IR photometry (see Section 3 of the main manuscript). Finally, all four fields are covered at radio wavelengths by the VLA as part of the FIRST survey.

A.4. A Color–Luminosity-matched Galaxy Sample

The three surveys considered here, i.e., SDSS, Boötes, and DEEP2, have independent photometric detection and spectroscopic selection criteria. For those survey regions with complete and homogeneous spectroscopic coverage, the limiting source magnitude in the SDSS, Boötes, and DEEP2 surveys is $r < 17.77$, $I < 20.5$, and $R < 24.1$ AB magnitudes, respectively. While these surveys select sources at roughly the same observed wavelengths, albeit with varying degrees of sensitivities, the large ranges in target redshifts result in the rest-frame selection being markedly different. In particular, the rest-frame UV selection of galaxies in DEEP2 results in good sensitivity toward blue star-forming galaxies, which is further enhanced by the ability to detect strong [O II]$\lambda 3727$ at $z < 1.4$. By contrast, this results in a loss of sensitivity toward red galaxies with similar masses to the blue sources that would otherwise be detected in DEEP2 at the same redshift; this is due mainly to changes in the overall spectral shape of the dominant stellar population between rest-frame B and R bands. Such selection effects have been previously investigated by Willmer et al. (2006) and Faber et al. (2007). Conversely to the DEEP2 selection, the rest-frame red optical selection of the SDSS survey will result in a marginally reduced sensitivity toward nearby faint blue galaxies and greater completeness toward red galaxies. Hence, to carry out a comparison of the AGN host-galaxy properties, these optical selection effects must be mitigated. Here, we build on the previous methodology of Blanton (2006) and describe our technique to perform K-corrections to the observed photometry and match the source catalogs based on their rest-frame optical measurements.

A.4.1. Galaxy K-corrections

We begin by performing standard optical K-corrections independently across the three surveys. For the Boötes (NDWFS) photometry, we convert Vega magnitudes to AB using corrections of: $B_W = +0.02$ mag, $R = +0.19$ mag, and $I = +0.44$ mag (e.g., Hickox et al. 2009). We also correct the SDSS and Boötes photometry for interstellar extinction (Schlegel et al. 1998). The photometry for DEEP2 is provided extinction-corrected in AB standard (Coil et al. 2004).

For this investigation, we are particularly interested in constraining the host-galaxy properties. Hence, we select all sources in Boötes and DEEP2 with $P_{gal} > 0.9$ (defined in Coil et al. 2004) to robustly remove stars and quasars (i.e., extremely luminous AGN that dominate the galaxy starlight). In the SDSS, sources are selected from the SDSS-DR7 galaxy catalog, which by design does not include Galactic sources or quasars (see Strauss et al. 2002; Richards et al. 2002). Photometric K-corrections are performed using the publicly available C and IDL tool, KCORRECT (v4.2).[16] KCORRECT fits a carefully chosen set of stellar population synthesis (e.g., Bruzual & Charlot 2003) and photoionization/shock (e.g., MAPPINGS-III; Sutherland & Dopita 1993) templates to the observed photometry, where the templates have been shifted to the known redshift of the source. In a standard implementation of KCORRECT, the best-fit template is then deprojected at rest frame to calculate the required K-correction for the survey photometric filters and/or produce the intrinsic photometry in custom filters defined for arbitrary redshifts. Such measurements can then be used to construct rest-frame color–magnitude diagrams for large source populations. However, here, we must first consider the inherent source selection bias in the SDSS, Boötes, and DEEP2 surveys, caused by the differing median source redshifts and the observed-frame selection techniques.

Sources identified in the spatial regions covered by Boötes and DEEP2 are observed with relatively similar *BRI* photometric filters. However, given the higher median redshift of the DEEP2 sample ($z \sim 0.87$) compared to that of Boötes ($z \sim 0.34$), this translates to sampling shorter and narrower rest-frame wavelengths for galaxies in DEEP2, particularly for the highest redshift sources. In principle, K-corrections derived for sources with three-band photometry covering only $\lambda \sim 2290$–4210 Å in the rest-frame (similar to the wavelength range covered by NUV$_{GALEX}$–U$_{Johnson}$) may fail to fit the majority of the reprocessed light due to foreground extinction, as well as failing to account for the starlight from old stellar populations, which typically emits at longer optical wavelengths. To partially mitigate these effects, we artificially over-sampled and extended

---

[16] The current version of KCORRECT is available at http://howdy.physics.nyu.edu/index.php/Kcorrect.

the photometric measurements to $\lambda \gtrsim 9000$ Å using the available DEIMOS spectroscopy.

For each DEEP2 galaxy, we predicted synthetic photometry in five predefined medium-band filters to supplement the standard *BRI* data during the KCORRECT fitting process. We constructed five relatively narrow (500 Å) filters that are based on the response shape of the r_{SDSS} filter, and centered at $\lambda_0 = \{6750, 7250, 7750, 8250, 8750$ Å$\}$. The DEIMOS spectra were convolved with the *I*-band filter and flux-calibrated using the *I*-band measurement after applying a simple aperture correction between the DEIMOS slit and the photometric aperture at the effective wavelength of the filter ($\lambda_{eff} \sim 8060$ Å). The individual source spectra were then convolved with the five constructed $I'_{1:5}$ filters, and synthetic spectral-photometric measurements were extracted. We note that the choice and use of five synthetic photometric points is somewhat arbitrary. However, we found that five additional photometric measurements can adequately map the depth of the D_{4000} break (visible at $z \sim 0.7$–1.2) in the galaxy spectra, which is primarily used to determine the stellar population contributions in synthesis modeling. We tested the use of five additional filters (for a total of seven filters) versus six and seven additional filters, and while we found that increasing numbers of photometric points can map the D_{4000} break and emission-line features with greater accuracy, the overall improvement to the χ-squared value was marginal. Due to the large number of spectra to be analyzed ($\sim 50,000$), we found that five additional narrow-band photometric points was an adequate trade-off between increasing accuracy and processing time.

K-corrections were calculated for the DEEP2 galaxies using the method outlined above and the $BRI'_{1:5}$ photometric measurements. Figure 8(a) shows an example KCORRECT fit to the $BRI'_{1:5}$ photometry for a typical $z \sim 0.9$ DEEP2 galaxy. The fitted KCORRECT template adequately reproduces the main features observed in the DEIMOS spectra, giving strong confidence that the calculated rest-frame photometry is appropriate for our purposes.

At $z > 1.1$, the measurement of the $^{0.1}g$-band magnitude becomes an extrapolation from the DEEP2 data. To assess what effect, if any, this has on the derived quantities from KCORRECT, we simulated several thousand galaxy spectra over the redshift range 0.6–1.5 using the SED galaxy templates of Polletta et al. (2007), which cover a range of galaxy types from the most massive elliptical systems to dwarf starburst galaxies. The Polletta et al. (2007) galaxy templates are not included as part of the KCORRECT spectral library. Hence, their use here can be considered a good independent test of the capabilities of KCORRECT and our methodology. As part of the simulations, we include low-level Poissonian noise at the 10% level for galaxies at $z = 0.6$ and increase the noise linearly by a factor $(1 + z)$ for galaxies to $z = 1.5$. We convolved these simulated spectra with the SDSS $^{0.1}g$-band filter (at $z = 0$), our synthetic $BRI'_{1:5}$ filter set (at the random simulated redshift), and the standard DEEP2 *BRI* filter set to produce the intrinsic and observed photometric quantities for the simulated sources. Using KCORRECT, we calculated the appropriate *K* corrections for each galaxy to find the fitted value for $^{0.1}m_g$ from the input photometry. Figure 8(b) shows the residuals of the fitted (KCORRECT-produced) and direct $^{0.1}m_g$ measurements for the simulated spectra as a function of redshift. We find that both the standard DEEP2 *BRI* and our synthetic $BRI'_{1:5}$ filters do a remarkably good job at reproducing the initial $^{0.1}m_g$ measurement to $z \sim 0.95$ with a relatively small 1σ dispersion

of ~ 0.015 mag over the full range of galaxy templates. In the same redshift range, the use of the standard *BRI* filters produces an extremely marginal overestimation of the $^{0.1}m_g$ brightness (-0.07 mags) for these simulated galaxies. At $z \sim 0.95$–1.1, we find a systematic underestimate of $+0.015$–0.03 mag in the median $^{0.1}m_g$ for the $BRI'_{1:5}$ filters. This appears to be driven by poor fits to galaxy types Scd and later. For these particular galaxies, this systematic offset increases to ~ 0.1 mag at $z = 1.4$. However, in actuality these relatively small and low-mass galaxies would be too faint to be selected in DEEP2 at this redshift. With the exception of the Scd and Sdm templates, we find no systematic offset across the entire redshift range considered here when using the $BRI'_{1:5}$ spectral photometry, with a maximum 1σ dispersion of $+0.07$ mag from the median, occurring at $z = 1.4$. As expected, the extrapolation of the $^{0.1}m_g$ measurement becomes more noticeable at $z > 1.1$ when only considering the *BRI* photometry. Due to the inability to robustly map the D_{4000} break and other spectral features, KCORRECT produces a systematic overestimate of $+0.14$ mag for galaxies simulated at $z = 1.4$, irrespective of galaxy type. However, it is worth noting that the use of only the *BRI* filters, which produce this observed offset, would have had little effect on any of the conclusions found throughout this manuscript, and this offset is well within the uncertainties for a source position in a rest-frame color–magnitude diagram.

A.4.2. Passive Evolution Corrections and Selection Matching

Using the best-fit rest-frame galaxy/AGN template determined for each source, we predicted if the source is sufficiently luminous at z_0 to be detected in the other two survey fields (e.g., is a particular SDSS galaxy sufficiently bright that it could have been detected in the Boötes and DEEP2 bandpasses). For each source, we use a Metropolis-Hastings sampler to randomly select two redshifts, z_1 and z_2, from the appropriate survey redshift distributions (i.e., from the two surveys that the source was not originally selected in) to be applied to the best-fit rest-frame template. We applied passive-evolution corrections to the source luminosity to shift the observed-frame KCORRECT-template at z_0 to z_1 and z_2. For those galaxies lying in the blue cloud of the color–magnitude diagram, we evolved the templates by $+0.98$ mag per unit redshift, and for red-sequence sources by$+0.66$ mag per unit redshift (Blanton 2006). The larger correction for the blue-cloud galaxies simultaneously includes a passive-evolution correction as well as accounting for the overall decline in the specific SFR in the last 9 Gyr. We also note here, that the use of a pseudo-random redshift for each source selected from the survey redshift distribution, as opposed to the redshift-limit of the survey, ensures a meaningful and realistic luminosity distribution for the galaxy population. Redshifted and luminosity-corrected source templates are then deprojected back into the observed-frame photometric filters for the survey bandpasses, and those sources that meet the selection criteria for all three surveys are included in the final-matched source sample.

For the galaxies identified in DEEP2, we found that the introduction of the synthetic $I'_{1:5}$ photometry, as part of the KCORRECT analysis (see Appendix A.4), significantly improved the quality of the template fitting, resulting in reduced uncertainties (on average by $\sim 85\%$ from the three-band DEEP2 data) in the inferred $^{0.1}u$- and $^{0.1}g$-band photometry. Furthermore, we observed that the wide spread in $^{0.1}(u$–$g)$ color (~ 0.5 mags) found for passive red-sequence DEEP2 galaxies (see Section 4.1) was not significantly decreased compared to using a single *I*-band photometric
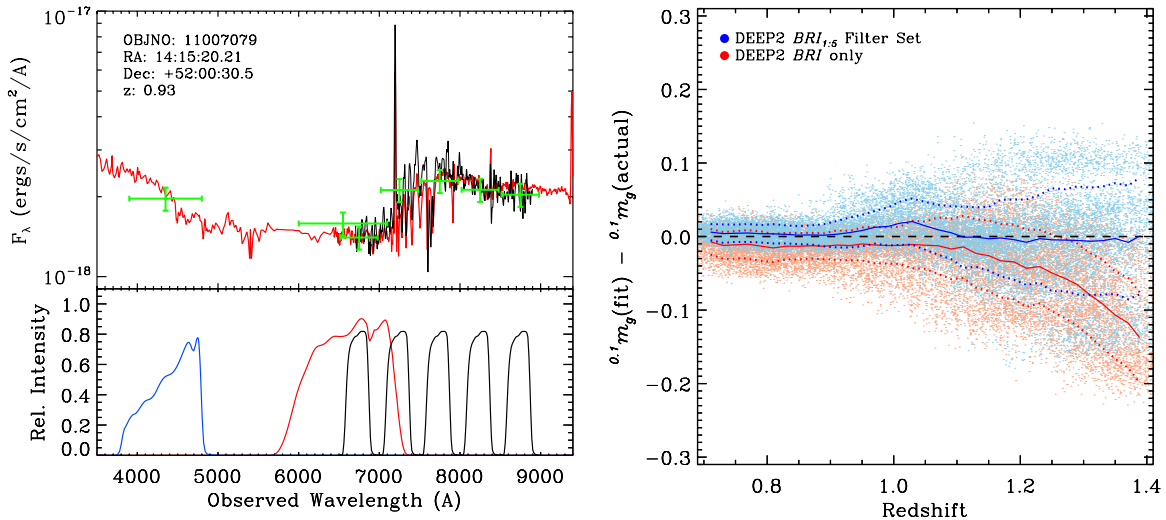
Figure 8. Left (top panel): example of a typical KCORRECT fit to a DEEP2 galaxy using the measured $BR + I'_{1:5}$ photometry (green points). Flux density as a function of observed wavelength is shown for the DEIMOS spectroscopy (black; Newman et al. 2013), stellar+photoionization+A_V template produced by KCORRECT is shown with red solid line. Lower panel: photometric responses for the standard DEEP2 B (blue) and R (red) filters, and our custom narrow I filters (black) used during the KCORRECT fitting procedure. Right: residuals of apparent g-band ($z = 0.1$) magnitude ($^{0.1}m_g$) as a function of source redshift produced by KCORRECT for the galaxy templates of Polletta et al. (2007). A random array of redshifts were applied to the spectral templates to construct photometry and produce K-corrections using our custom $BRI'_{1:5}$ filters (blue dots) and the standard DEEP2 BRI filters (red dots). Median residuals and associated 1σ dispersion about the median are shown for both sets of simulations with solid and dotted lines, respectively.

(A color version of this figure is available in the online journal.)

point. This suggests that other systematic effects may dominate the KCORRECT fitting process and/or the red sequence is intrinsically broader in $^{0.1}(u–g)$ color at higher-redshift. However, further analysis of the intrinsic color–magnitude distribution at $z \sim 1$ is beyond the scope of this investigation and is arguably not suited to only the three-band BRI photometry available in DEEP2.

Finally, we note that we have not attempted to correct for potential biases resulting from the requirement of a spectroscopic redshift for each source. For example, galaxies lacking emission lines or other obvious emission features that would be used to discern a redshift will be uniformly selected against across our entire galaxy sample. Given that we have tailored the galaxy selection to the redshift regimes where the individual surveys are most sensitive, this bias will most likely affect the low-luminosity end of each sample and not the galaxies hosting luminous AGN. Furthermore, while less of a potential issue due to repeat exposures and observations shifting/dithering, galaxies with very close-by neighbors as projected onto the sky may be systematically avoided or result in redshift failures due to blending effects.

REFERENCES

Abazajian, K. N., Adelman-McCarthy, J. K., Agüeros, M. A., et al. 2009, ApJS, 182, 543
Aird, J., Coil, A. L., Moustakas, J., et al. 2012, ApJ, 746, 90
Alexander, D. M., Bauer, F. E., Brandt, W. N., et al. 2011, ApJ, 738, 44
Alexander, D. M., Chary, R., Pope, A., et al. 2008, ApJ, 687, 835
Alexander, D. M., & Hickox, R. C. 2012, NewAR, 56, 93
Alexander, D. M., Smail, I., Bauer, F. E., et al. 2005, Natur, 434, 738
Ashby, M. L. N., Stern, D., Brodwin, M., et al. 2009, ApJ, 701, 428
Ashby, M. L. N., Willner, S. P., Fazio, G. G., et al. 2013, ApJ, 769, 80
Baldry, I. K., Glazebrook, K., Brinkmann, J., et al. 2004, ApJ, 600, 681
Barger, A. J., Cowie, L. L., Mushotzky, R. F., et al. 2005, AJ, 129, 578
Barmby, P., Huang, J.-S., Ashby, M. L. N., et al. 2008, ApJS, 177, 431
Becker, R. H., White, R. L., & Helfand, D. J. 1995, ApJ, 450, 559
Becker, R. H., White, R. L., Helfand, D. J., & Zoonematkermani, S. 1994, ApJS, 91, 347
Bell, E. F., McIntosh, D. H., Katz, N., & Weinberg, M. D. 2003, ApJS, 149, 289
Bell, E. F., Wolf, C., Meisenheimer, K., et al. 2004, ApJ, 608, 752
Bertin, E., & Arnouts, S. 1996, A&AS, 117, 393
Best, P. N., Kauffmann, G., Heckman, T. M., et al. 2005, MNRAS, 362, 25
Blanton, M. R. 2006, ApJ, 648, 268
Blanton, M. R., Brinkmann, J., Csabai, I., et al. 2003a, AJ, 125, 2348
Blanton, M. R., Hogg, D. W., Bahcall, N. A., et al. 2003b, ApJ, 594, 186
Blanton, M. R., & Roweis, S. 2007, AJ, 133, 734
Bonfield, D. G., Jarvis, M. J., Hardcastle, M. J., et al. 2011, MNRAS, 416, 13
Bongiorno, A., Merloni, A., Brusa, M., et al. 2012, MNRAS, 427, 3103
Borch, A., Meisenheimer, K., Bell, E. F., et al. 2006, A&A, 453, 869
Bower, R. G., Benson, A. J., & Crain, R. A. 2012, MNRAS, 422, 2816
Bower, R. G., Benson, A. J., Malbon, R., et al. 2006, MNRAS, 370, 645
Bower, R. G., McCarthy, I. G., & Benson, A. J. 2008, MNRAS, 390, 1399
Brand, K., Brown, M. J. I., Dey, A., et al. 2006, ApJ, 641, 140
Brinchmann, J., Charlot, S., White, S. D. M., et al. 2004, MNRAS, 351, 1151
Bruzual, G., & Charlot, S. 2003, MNRAS, 344, 1000
Cardamone, C. N., Urry, C. M., Schawinski, K., et al. 2010, ApJL, 721, L38
Chen, C.-T. J., Hickox, R. C., Alberts, S., et al. 2013, ApJ, 773, 3
Cisternas, M., Jahnke, K., Bongiorno, A., et al. 2011, ApJL, 741, L11
Coil, A. L., Blanton, M. R., Burles, S. M., et al. 2011, ApJ, 741, 8
Coil, A. L., Georgakakis, A., Newman, J. A., et al. 2009, ApJ, 701, 1484
Coil, A. L., Newman, J. A., Kaiser, N., et al. 2004, ApJ, 617, 765
Condon, J. J. 1992, ARA&A, 30, 575
Cooper, M. C., Newman, J. A., Croton, D. J., et al. 2006, MNRAS, 370, 198
Croton, D. J., Springel, V., White, S. D. M., et al. 2006, MNRAS, 365, 11
Cuillandre, J.-C., Luppino, G., Starr, B., & Isani, S. 2001, in SF2A-2001: Semaine de l'Astrophysique Francaise, ed. F. Combes, D. Barret, & F. Thévenin (San Francisco, CA: ASP), 605
D'Abrusco, R., Massaro, F., Paggi, A., et al. 2013, ApJS, 206, 12
Davis, M., Faber, S. M., Newman, J., et al. 2003, Proc. SPIE, 4834, 161
Davis, M., Guhathakurta, P., Konidaris, N. P., et al. 2007, ApJL, 660, L1
de Vries, W. H., Morganti, R., Röttgering, H. J. A., et al. 2002, AJ, 123, 1784
Di Matteo, T., Springel, V., & Hernquist, L. 2005, Natur, 433, 604
Dole, H., Lagache, G., Puget, J.-L., et al. 2006, A&A, 451, 417
Donley, J. L., Koekemoer, A. M., Brusa, M., et al. 2012, ApJ, 748, 142
Donley, J. L., Rieke, G. H., Alexander, D. M., Egami, E., & Pérez-González, P. G. 2010, ApJ, 719, 1393
Donley, J. L., Rieke, G. H., Pérez-González, P. G., & Barro, G. 2008, ApJ, 687, 111
Donley, J. L., Rieke, G. H., Rigby, J. R., & Pérez-González, P. G. 2005, ApJ, 634, 169
Dunlop, J. S., McLure, R. J., Kukula, M. J., et al. 2003, MNRAS, 340, 1095
Eisenhardt, P. R., Stern, D., Brodwin, M., et al. 2004, ApJS, 154, 48
Evans, I. N., Primini, F. A., Glotfelty, K. J., et al. 2010, ApJS, 189, 37
Faber, S. M., Willmer, C. N. A., Wolf, C., et al. 2007, ApJ, 665, 265

Fabian, A. C. 2012, ARA&A, 50, 455
Fabricant, D., Fata, R., Roll, J., et al. 2005, PASP, 117, 1411
Fazio, G. G., Hora, J. L., Allen, L. E., et al. 2004, ApJS, 154, 10
Frayer, D. T., Huynh, M. T., Chary, R., et al. 2006, ApJL, 647, L9
Gabor, J. M., & Bournaud, F. 2013, MNRAS, 434, 606
Georgakakis, A., Coil, A. L., Laird, E. S., et al. 2009, MNRAS, 397, 623
Georgakakis, A., & Nandra, K. 2011, MNRAS, 414, 992
Georgantopoulos, I., Comastri, A., Vignali, C., et al. 2013, A&A, 555, 43
Gerke, B. F., Newman, J. A., Davis, M., et al. 2012, ApJ, 751, 50
Goulding, A. D., & Alexander, D. M. 2009, MNRAS, 398, 1165
Goulding, A. D., Alexander, D. M., Bauer, F. E., et al. 2012a, ApJ, 755, 5
Goulding, A. D., Alexander, D. M., Lehmer, B. D., & Mullaney, J. R. 2010, MNRAS, 406, 597
Goulding, A. D., Forman, W. R., Hickox, R. C., et al. 2012b, ApJS, 202, 6
Guainazzi, M., Matt, G., & Perola, G. C. 2005, A&A, 444, 119
Hasinger, G., Miyaji, T., & Schmidt, M. 2005, A&A, 441, 417
Heckman, T. M., Kauffmann, G., Brinchmann, J., et al. 2004, ApJ, 613, 109
Hickox, R. C., Jones, C., Forman, W. R., et al. 2009, ApJ, 696, 891
Hickox, R. C., Mullaney, J. R., Alexander, D. M., et al. 2014, ApJ, 782, 9
Hogg, D. W., Blanton, M. R., Eisenstein, D. J., et al. 2003, ApJL, 585, L5
Hopkins, P. F., Cox, T. J., Kereš, D., & Hernquist, L. 2008, ApJS, 175, 390
Hopkins, P. F., & Elvis, M. 2010, MNRAS, 401, 7
Hopkins, P. F., Hickox, R., Quataert, E., & Hernquist, L. 2009, MNRAS, 398, 333
Hopkins, P. F., Richards, G. T., & Hernquist, L. 2007, ApJ, 654, 731
Ivison, R. J., Chapman, S. C., Faber, S. M., et al. 2007, ApJL, 660, L77
Jannuzi, B. T., & Dey, A. 1999, in ASP Conf. Ser. 191, Photometric Redshifts and the Detection of High Redshift Galaxies, ed. R. Weymann, L. Storrie-Lombardi, M. Sawicki, & R. Brunner (San Francisco: CA: ASP) 111
Jones, C., Churazov, E., Giacintucci, S., et al. 2010, in AIP Conf. Proc. 1248, X-ray Astronomy 2009; Present Status, Multi-Wavelength Approach and Future Perspectives, ed. A. Comastri, L. Angelini, & M. Cappi (Melville, NY: AIP), 253
Juneau, S., Dickinson, M., Alexander, D. M., & Salim, S. 2011, ApJ, 736, 104
Juneau, S., Dickinson, M., Bournaud, F., et al. 2013, ApJ, 764, 176
Kauffmann, G., & Heckman, T. M. 2009, MNRAS, 397, 135
Kauffmann, G., Heckman, T. M., & Best, P. N. 2008, MNRAS, 384, 953
Kauffmann, G., Heckman, T. M., Tremonti, C., et al. 2003a, MNRAS, 346, 1055
Kauffmann, G., Heckman, T. M., White, S. D. M., et al. 2003b, MNRAS, 341, 33
Kauffmann, G., Heckman, T. M., White, S. D. M., et al. 2003c, MNRAS, 341, 54
Kenter, A., Murray, S. S., Forman, W. R., et al. 2005, ApJS, 161, 9
Kocevski, D. D., Faber, S. M., Mozena, M., et al. 2012, ApJ, 744, 148
Kochanek, C. S., Eisenstein, D. J., Cool, R. J., et al. 2012, ApJS, 200, 8
Kormendy, J., & Ho, L. C. 2013, arXiv e-prints
Lacy, M., Storrie-Lombardi, L. J., Sajina, A., et al. 2004, ApJS, 154, 166
Laird, E. S., Nandra, K., Georgakakis, A., et al. 2009, ApJS, 180, 102
LaMassa, S. M., Heckman, T. M., Ptak, A., et al. 2009, ApJ, 705, 568
LaMassa, S. M., Heckman, T. M., Ptak, A., et al. 2012, ApJ, 758, 1
LaMassa, S. M., Heckman, T. M., Ptak, A., & Urry, C. M. 2013, ApJL, 765, L33
Lira, P., Ward, M., Zezas, A., Alonso-Herrero, A., & Ueno, S. 2002, MNRAS, 330, 259
Lutz, D., Mainieri, V., Rafferty, D., et al. 2010, ApJ, 712, 1287
Lutz, D., Sturm, E., Tacconi, L. J., et al. 2008, ApJ, 684, 853
Magorrian, J., Tremaine, S., Richstone, D., et al. 1998, AJ, 115, 2285
Marchesini, D., van Dokkum, P. G., Förster Schreiber, N. M., et al. 2009, ApJ, 701, 1765
Martínez-Sansigre, A., Rawlings, S., Bonfield, D. G., et al. 2007, MNRAS, 379, L6
Mateos, S., Alonso-Herrero, A., Carrera, F. J., et al. 2012, MNRAS, 426, 3271
McNamara, B. R., & Nulsen, P. E. J. 2007, ARA&A, 45, 117
Menci, N., Fiore, F., Puccetti, S., & Cavaliere, A. 2008, ApJ, 686, 219
Mendez, A. J., Coil, A. L., Aird, J., et al. 2013, ApJ, 770, 40
Moran, E. C., Lehnert, M. D., & Helfand, D. J. 1999, ApJ, 526, 649
Moustakas, J., Coil, A. L., Aird, J., et al. 2013, ApJ, 767, 50
Mullaney, J. R., Alexander, D. M., Fine, S., et al. 2013, MNRAS, 433, 622
Mullaney, J. R., Pannella, M., Daddi, E., et al. 2012, MNRAS, 419, 95
Murray, S. S., Kenter, A., Forman, W. R., et al. 2005, ApJS, 161, 1
Nandra, K., Georgakakis, A., Willmer, C. N. A., et al. 2007, ApJL, 660, L11
Nandra, K., Laird, E. S., Adelberger, K., et al. 2005, MNRAS, 356, 568
Newman, J. A., Cooper, M. C., Davis, M., et al. 2013, ApJS, 208, 5
Novak, G. S., Ostriker, J. P., & Ciotti, L. 2011, ApJ, 737, 26
Page, M. J., Stevens, J. A., Ivison, R. J., & Carrera, F. J. 2004, ApJL, 611, L85
Park, S. Q., Barmby, P., Willner, S. P., et al. 2010, ApJ, 717, 1181
Peacock, J. A. 1983, MNRAS, 202, 615
Polletta, M., Trajer, M., Maraschi, L., et al. 2007, ApJ, 663, 81
Rafferty, D. A., McNamara, B. R., Nulsen, P. E. J., & Wise, M. W. 2006, ApJ, 652, 216
Richards, G. T., Fan, X., Newberg, H. J., et al. 2002, AJ, 123, 2945
Richards, G. T., Strauss, M. A., Fan, X., et al. 2006, AJ, 131, 2766
Rosario, D. J., Mozena, M., Wuyts, S., et al. 2013, ApJ, 763, 59
Rosario, D. J., Santini, P., Lutz, D., et al. 2012, A&A, 545, A45
Ross, N. P., McGreer, I. D., White, M., et al. 2013, ApJ, 773, 14
Sarajedini, V. L., Koo, D. C., Klesman, A. J., et al. 2011, ApJ, 731, 97
Schawinski, K., Evans, D. A., Virani, S., et al. 2010, ApJL, 724, L30
Schawinski, K., Kaviraj, S., Khochfar, S., et al. 2007a, ApJS, 173, 512
Schawinski, K., Simmons, B. D., Urry, C. M., Treister, E., & Glikman, E. 2012, MNRAS, 425, L61
Schawinski, K., Thomas, D., Sarzi, M., et al. 2007b, MNRAS, 382, 1415
Schawinski, K., Treister, E., Urry, C. M., et al. 2011, ApJL, 727, L31
Schlegel, D. J., Finkbeiner, D. P., & Davis, M. 1998, ApJ, 500, 525
Shao, L., Kauffmann, G., Li, C., Wang, J., & Heckman, T. M. 2013, MNRAS, 436, 3451
Smolčić, V. 2009, ApJL, 699, L43
Smolčić, V., Zamorani, G., Schinnerer, E., et al. 2009, ApJ, 696, 24
Stern, D., Eisenhardt, P., Gorjian, V., et al. 2005, ApJ, 631, 163
Strateva, I., Ivezić, Ž., Knapp, G. R., et al. 2001, AJ, 122, 1861
Strauss, M. A., Weinberg, D. H., Lupton, R. H., et al. 2002, AJ, 124, 1810
Sutherland, R. S., & Dopita, M. A. 1993, ApJS, 88, 253
Symeonidis, M., Kartaltepe, J., Salvato, M., et al. 2013, MNRAS, 433, 1015
Tozzi, P., Gilli, R., Mainieri, V., et al. 2006, A&A, 451, 457
Tremaine, S., Gebhardt, K., Bender, R., et al. 2002, ApJ, 574, 740
Tremonti, C. A., Heckman, T. M., Kauffmann, G., et al. 2004, ApJ, 613, 898
Trump, J. R., Konidaris, N. P., Barro, G., et al. 2013, ApJL, 763, L6
Ueda, Y., Akiyama, M., Ohta, K., & Miyaji, T. 2003, ApJ, 598, 886
Wake, D. A., Croom, S. M., Sadler, E. M., & Johnston, H. M. 2008, MNRAS, 391, 1674
Wilkes, B. J., Kuraszkiewicz, J., Haas, M., et al. 2013, ApJ, 773, 15
Willmer, C. N. A., Faber, S. M., Koo, D. C., et al. 2006, ApJ, 647, 853
Willner, S. P., Ashby, M. L. N., Barmby, P., et al. 2012, ApJ, 756, 72
Wright, E. L., Eisenhardt, P. R. M., Mainzer, A. K., et al. 2010, AJ, 140, 1868
Xue, Y. Q., Brandt, W. N., Luo, B., et al. 2010, ApJ, 720, 368
Yan, L., Donoso, E., Tsai, C.-W., et al. 2013, AJ, 145, 55
York, D. G., Adelman, J., Anderson, J. E., Jr, et al. 2000, AJ, 120, 1579